



Planktonic foraminiferal assemblages as tracers of paleoceanographic changes within the northern Benguela current system since the Early Pleistocene

Arianna V. Del Gaudio¹, Aaron Avery², Gerald Auer¹, Werner E. Piller¹, and Walter Kurz¹

¹Department of Earth Sciences (Geology and Paleontology), NAWI Graz Geocenter, University of Graz, 8010 Graz, Austria

²School of Geosciences, University of South Florida, Tampa, FL 33620, USA

Correspondence: Arianna V. Del Gaudio (arianna.del-gaudio@uni-graz.at)

Received: 4 March 2024 – Discussion started: 18 March 2024

Revised: 4 August 2024 – Accepted: 14 August 2024 – Published: 9 October 2024

Abstract. The Benguela Upwelling System (BUS), located in the southeastern Atlantic Ocean, represents one of the world's most productive regions. This system is delimited to the south by the Agulhas retroflexion region. The northern boundary of the BUS is, instead, represented by the Angola–Benguela Front (ABF), which is a thermal feature separating warm waters of the Angola Basin (including the South Atlantic Central Water; SACW) from the cooler Benguela Oceanic Current (BOC). We performed statistical analyses on planktonic foraminiferal assemblages in 94 samples from Holes U1575A and U1576A, cored during International Ocean Discovery Program (IODP) Expedition 391. Drilled sites are located along the Tristan–Gough–Walvis Ridge (TGW) seamount track in the northern sector of the BUS (offshore the Namibian continental margin). The analyzed stratigraphic intervals span the Early–Late Pleistocene, marked by the Early–Middle Pleistocene transition (EMPT; 1.40–0.40 Myr), during which important glacial–interglacial sea surface temperature (SST) variabilities occurred. This work provides novel insights on the local paleoceanographic evolution of the northern BUS and associated thermocline variability based on the ecological significance of the foraminiferal assemblages. Specifically, variations in the assemblage content allowed us to characterize the different water masses (BOC, SACW, and Agulhas waters) and reconstruct their interactions during the Quaternary. The interplay of the previously mentioned water masses induced perturbations in the BUS (ABF latitudinal shifts and input of tropical waters from the Agulhas retroflex-

ion region). Furthermore, we investigated the possible link between changes in the paleoceanographic conditions and climatic events (e.g., Benguela Niño-/Niña-like phases and deglaciation stages) recorded since the EMPT.

1 Introduction

The Benguela Upwelling System (BUS) in the southeastern Atlantic Ocean is known as one of the key temperate productive regions on Earth (Giraudeau, 1992; Little et al., 1997; Petrick et al., 2018) since the Middle Miocene (Diester-Haass, 1988). This area is, in fact, subjected to strong upwelling episodes, during which cold and nutrient-enriched subsurface waters rise to the surface along the southeastern coast of the African continent (Giraudeau, 1992; Little et al., 1997; Ufkes and Kroon, 2009; Rouault and Tomety, 2022). Interestingly, the BUS is also influenced by the ingression of warm Indian Ocean waters (so-called Agulhas Leakage) via Agulhas eddies (Bé and Duplessy, 1976; Fine et al., 1988; Caley et al., 2012) and by the subsurface South Atlantic Central Water (SACW) from the Angola Basin (Mohrholz et al., 2008; Ufkes and Kroon, 2012). The meridional thermal front, which forms in the convergence zone between the warm subsurface waters and the cold Benguela waters, is called the Angola–Benguela Front (ABF; Mohrholz et al., 2008; Kopte et al., 2017).

Modern reconstructions (e.g., Gammelsrød et al., 1998; Rouault et al., 2007) of sea surface temperatures (SSTs)

within the BUS also reveal the existence of a strong inter-annual SST variability, which induces severe warm (cold) events along the Angola–Namibia coast known as Benguela Niño (Benguela Niña) events (Shannon et al., 1986; Imbol Koungue et al., 2019). These climatic phenomena severely affect the paleoceanographic conditions in the BUS (e.g., the position of the ABF; Walter, 1937; Boyd et al., 1987; Shannon and Nelson, 1996). Several studies suggested the occurrence of Benguela Niño/Niña events during the Pliocene–Pleistocene time intervals (e.g., Ufkes and Kroon, 2012; Rosell-Melé et al., 2014). In particular, since the onset of the Early–Middle Pleistocene transition (EMPT), a strong glacial–interglacial sea surface temperature (SST) variability occurred, possibly promoting the development of Benguela Niño/Niña conditions (Herbert, 2023).

In this study, we analyzed planktonic foraminiferal assemblages during and after the EMPT to investigate the paleoceanographic history of the most distal sector of the BUS, offshore the South African continental margin. Previous studies (e.g., Little et al., 1997; Giraudeau, 1993; West et al., 2004) mainly analyzed planktonic foraminiferal assemblages in younger sediment cores close to the continental margin, thus principally focusing on the coastal upwelling system. Moreover, Ufkes and Kroon (2012) investigated the paleoecological conditions of the BUS in the last 1.1 Ma, not covering the whole EMPT interval. International Ocean Discovery Program (IODP) Expedition 391 Sites U1575 and U1576 were drilled along the Tristan–Gough–Walvis Ridge (TGW) seamount track in the northern Benguela region, under the influence of the Benguela Oceanic Current (BOC) and close to the ABF (Figs. 1 and 2). The location of the sites is ideal for detecting regional changes in the paleoceanographic conditions within the distal part of the BUS and for exploring the interaction of the BOC with the Angola Basin and Indian Ocean water masses. Furthermore, the sites were cored in different sectors of the South Atlantic Gyre system (SAGS), with Hole U1575A located near the continental margin and Hole U1576A situated in a more southern position and closer to the center of the gyre (Fig. 2). This allowed us to infer variations of the paleoceanographic conditions in different parts of the SAGS.

The major objectives of our study were to (1) characterize the BOC, the SACW, and the Agulhas Leakage in terms of planktonic foraminiferal assemblage compositions; (2) examine the interaction of the BOC with the warm waters from the Angola Basin (which affects the ABF position) and the Indian Ocean waters (through Agulhas Leakage) during the Quaternary; (3) detect the response of the regional thermocline to the variations in the paleoecological conditions in the area; and (4) investigate the link between changes in the ABF position and in the influx of the Agulhas waters to climatic conditions (e.g., Benguela Niño/Niña-like events and deglaciation phases), which were previously documented to have occurred since the onset of the EMPT.

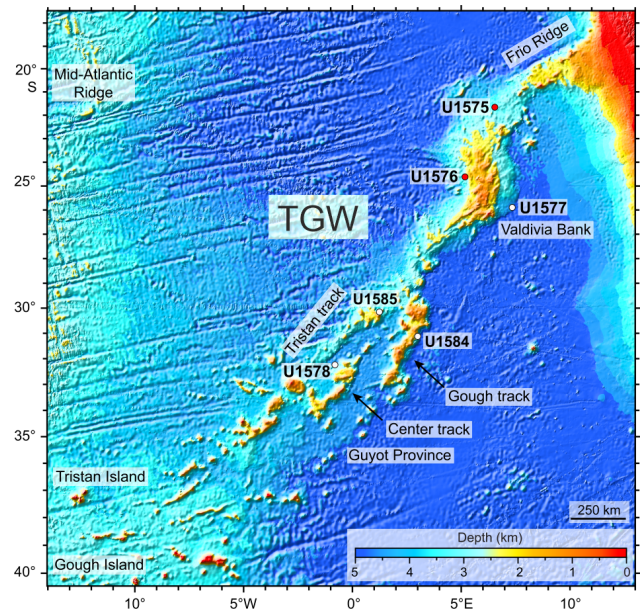


Figure 1. Bathymetric map of the Tristan–Gough–Walvis Ridge (TGW) volcanic chain and its main seamount tracks (modified from Sager et al., 2023). Red dots are the IODP sites used for this study.

1.1 Geological setting

The Tristan–Gough–Walvis Ridge (TGW) track is a volcanic chain in the eastern South Atlantic Ocean between 18 and 32° S (Humphris and Thompson, 1982; Sager et al., 2022; Fig. 1). It extends for 3100 km from Tristan da Cunha and Gough Island to the Namibian coast (Cape Frio) in southwestern Africa (Connary, 1972; Sager et al., 2020, 2022). Additionally, the ridge complex separates the Cape Basin in the south from the Angola Basin in the north (Shaffer, 1984). The TGW shows a complex morphology (Connary, 1972; Humphris and Thompson, 1982; Thoram et al., 2023), as it is formed by three seamount chains (Tristan Track, Central Track, and Gough Track) exhibiting different Pb isotopic compositions (Hoernle et al., 2000; Werner et al., 2003; Hoernle et al., 2015; Homrighausen et al., 2019; Sager et al., 2020). The TGW also comprises a continuous ridge (Frio Ridge), an oceanic plateau (Valdivia Bank), guyots, and scattered seamounts (Sager et al., 2020). The formation of the TGW started in the Early Cretaceous (~132 Ma), and it is related to the initial rifting of the South Atlantic Ocean. Some researchers (Wilson, 1965; Morgan, 1971; Detrick and Watts, 1979) suggested that the TGW was formed due to the lithospheric plate movement above a fixed hotspot. However, more recent studies (Fairhead and Wilson, 2005; Foulger, 2007) proposed that its origination could be linked to non-hotspot-related volcanism along shear zones (Sager et al., 2022).

Sites drilled along the TGW during IODP Expedition 391 (U1575, U1576, U1577, and U1578) recovered Upper Cre-

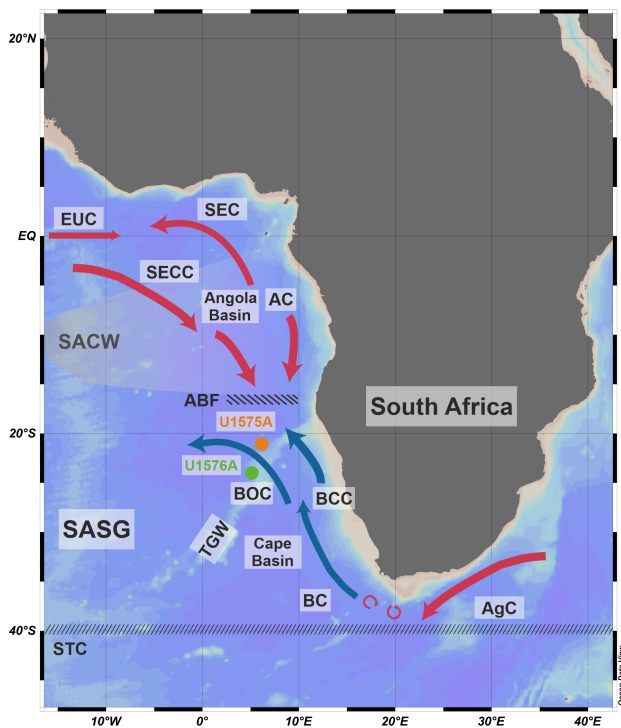


Figure 2. Oceanographic setting of the studied area (adapted from Ufkes and Kroon, 2012). The map was created using Ocean Data View (Schlitzer, 2021). Orange and green dots are the locations of Holes U1575A and U1576A. Red arrows are warm-water currents, blue arrows are cold-water currents, and circular arrows are Agulhas eddies. Oceanic features and the names of the water currents are abbreviated as follows. ABF: Angola–Benguela Front; AC: Angola Current; AgC: Agulhas Current; BC: Benguela Current; BCC: Benguela Coastal Current; BOC: Benguela Oceanic Current; EUC: Equatorial Undercurrent; SACW: South Atlantic Central Water; SASG: South Atlantic Subtropical Gyre; SEC: South Equatorial Current; SECC: South Equatorial Countercurrent; STC: Subtropical Convergence; TGW: Tristan–Gough–Walvis Ridge.

taceous (Campanian–Maastrichtian) to Upper Pleistocene sedimentary sequences (Sager et al., 2022). Main lithologies include white to pale-brown calcareous nannofossil–planktonic foraminifera oozes and brown–pink and light–green to gray nannofossil–foraminifera chalks, seldom interbedded with light- to dark-gray tephra layers.

1.2 Oceanographic setting

Holes U1575A and U1576A are situated in the eastern sector of the South Atlantic Subtropical Gyre (SASG; Fig. 2). The SASG is a wind-driven, counterclockwise flow, which is responsible for the redistribution of energy between low and high latitudes, thus controlling the global climate system (Gordon, 1973; Talley, 2003; Drouin et al., 2021; Pinho et al., 2021). It extends roughly between 45–15° S and 55° W–10° E (Drouin et al., 2021). Four major water masses define

the SASG, with the Benguela Current (BC) representing the eastern sector of the gyre (Stramma and Peterson, 1990; Garzoli and Gordon, 1996; Stramma and England, 1999; Fig. 2).

The Benguela Upwelling System (BUS), located along the southern African continental margin, is known as one of the most productive regions in the oceans (Rouault and Tomety, 2022), in which the southerly trade winds induce upwelling of cold, nutrient-rich subsurface waters along the western side of South Africa and Namibia (Giraudeau, 1992; Little et al., 1997; Ufkes and Kroon, 2012). The strength of the upwelling episodes and their seaward expansion are linked to wind stress (Lutjeharms and Meeuwis, 1987; Ufkes and Kroon, 2012) and glacial–interglacial fluctuations (Rosell-Melé et al., 2014). The BUS comprises northern, central, and southern areas which differ from the duration of the upwelling and the level of productivity (Lutjeharms and Stockton, 1987; Ufkes et al., 2000; Petrick et al., 2015). Specifically, the northern and central areas (north of 30° S) are characterized by perennial upwelling and high productivity (Andrews and Hutchings, 1980; Lutjeharms and Stockton, 1987; Hutchings et al., 2009), with upwelled cold and high-nutrient waters extending offshore in filaments (Rosell-Melé et al., 2014). Conversely, the southern area (south of 30° S) experiences periodical (seasonal) upwelling events and low nutrient levels (Andrews and Hutchings, 1980; Rosell-Melé et al., 2014; Petrick et al., 2015). The BUS is strictly linked to the Benguela Oceanic Current (BOC) and the Benguela Coastal Current (BCC) (Fig. 2; Little et al., 1997; Rosell-Melé et al., 2014). The BOC is a cold surface water mass that flows along the African coast from Cape Town (34° S) to Walvis Bay (23° S). When reaching ~ 23° S, the BOC diverges to the west at the TGW, while its coastal branch (the BCC) continues to move northwards towards the Angola region (Little et al., 1997).

The boundaries of the BUS are represented by the retroflexion region of the Agulhas Current (AgC) in the south and by the Angola–Benguela Front (ABF) in the north (Fig. 2; Little et al., 1997). The AgC is a warm and saline current which flows along the eastern margin of Africa, bringing Indian Ocean waters to the South Atlantic Ocean (Bé and Duplessy, 1976; Olson and Evans, 1986; Fine et al., 1988; Petrick et al., 2015). Specifically, the AgC does not reach the southeastern Atlantic region but retroreflects near the Cape Basin due to the westerlies stress curl (Lutjeharms, 1981; Petrick et al., 2015). AgC retroflexion eddies (rings) of warmer and saline waters then leak into the BUS, moving northwest (Petrick et al., 2015). This influx of AgC waters from the Indian Ocean is known as Agulhas Leakage (Fine et al., 1988; Petrick et al., 2015; Friesenhagen, 2022). A greater input of the Indian Ocean subtropical waters is induced by the increase in strength of the BOC (Garzoli et al., 1996). Conversely, the northward fluctuations of the cold Antarctic Circumpolar Current (ACC) result in a weaker leakage (McClymont et al., 2005; McIntyre et al., 1989; Peeters et al., 2004).

North of the BUS, the tropical warm and oligotrophic Angola Current (AC) flows poleward down to about 16° S, where it encounters the cool and nutrient-rich waters of the Benguela system, producing a thermal front known as the Angola–Benguela Front (ABF) (Fig. 2; Mohrholz et al., 2008; Kopte et al., 2017). The northern sector of the ABF is occupied by low-oxygen and high-saline subsurface waters (100–500 m water depth) named South Atlantic Central Water (SACW; Mohrholz et al., 2008; Ufkes and Kroon, 2012).

2 Materials and methods

The studied sites (U1575 and U1576) were cored during IODP Expedition 391, along the TGW Ridge seamount track, following a NE–SW transect. Lithological descriptions of the investigated sites mentioned below are from Sager et al. (2022). Sample depths are indicated as drilling depth below the seafloor (CSF-B, specified as m b.s.f.) to avoid core overlaps originating from core expansion on deck, resulting in a recovery of more than 100 % (as occurred in Hole U1576A).

Hole U1575A (21°51.9659' S, 06°35.4369' E; 3231.3 m water depth) is situated on the northwestern side of the Walvis Ridge, between Frio Ridge and Valdivia Bank (Fig. 1), and near the Namibian continental margin. Moreover, the site is located in the northernmost sector of the BUS (~17–25° S), under the influence of the BOC. The Pleistocene succession at this hole is represented by unconsolidated calcareous nannofossil–foraminiferal oozes (Lithostratigraphic Unit 1; 0–~40 m b.s.f.; Fig. 3). Gray-white and green bandings were recorded within the unit due to the accumulation of pyrite framboids and Fe–Mn-rich particles.

Hole U1576A (24°35.7520' S, 05°7.3163' E) was retrieved on the western side of the Valdivia Bank volcanic edifice at a water depth of 3032.3 m (Fig. 1). As for Site U1575, this hole is situated in the northern area of the BUS, within the latitudinal band of the BOC. The recovered Pleistocene sequence consists of part of Unit 1 (0 to ~45 m b.s.f.), separated into subunits 1A and 1B, based on different sediment colors and subtle changes in clay content. Subunit 1A is composed of pale-brown nannofossil–foraminiferal oozes, while subunit 1B is dominated by white nannofossil–foraminiferal oozes (Fig. 3).

2.1 Sample preparation

A total of 53 (Hole U1575A) and 41 (Hole U1576A) samples were prepared for biostratigraphic and quantitative analyses of the planktonic foraminiferal assemblage. The sediment was dried overnight at 40 °C, using an electric oven. Subsequently, the dried sediment was soaked in distilled water and then wet-sieved into four size fractions (63–125, 125–250, 250–500, and greater than 500 µm). In order to prevent contamination, all sieves were cleaned with methylene blue to recognize foraminiferal specimens from a previ-

ous wash. Once dried at 40–50 °C, the sediment was transferred into labeled glass vials (Haynes, 1981; Snyder and Huber, 1996; Arrigoni et al., 2023). Thereafter, planktonic specimens were observed using a ZEISS Discovery.V8 stereomicroscope and picked in the 125–500 µm size fractions. A ZEISS DSM 982 (Gemini) scanning electron microscope (SEM) was used to better assess the state of preservation of planktonic foraminifera and to image the most relevant taxa (see Plates A1 and B1–5).

Calcareous nannofossils were analyzed in 61 samples and solely used for biostratigraphic investigations at the studied sites. The simple smear slide technique (e.g., Haq and Lohmann, 1976; Backman and Shackleton, 1983; Bown and Young, 1998) was performed to obtain microslides. Untreated sediment and a few drops of distilled water were mixed to create a suspension which was subsequently smeared on a coverslip with the use of a toothpick. The coverslip was then dried at ~50 °C on a hotplate. Norland Optical Adhesive was utilized to mount the microslides. After preparation, slides were scanned for calcareous nannofossil content with a standard light microscope, ZEISS Axio Lab.A1, at 1000× magnification. Thereafter, individuals were imaged using an Axioplan 2 light microscope and a Leica DFC320 camera (see Plates A1 and B1–5). SEM analysis was additionally performed to detect the presence of small-sized coccoliths (e.g., *Emiliania huxleyi*).

2.2 Taxonomic remarks

2.2.1 Planktonic foraminifera

The taxonomy of planktonic foraminifera is largely derived from Blow (1969), Postuma (1971), Rögl (1974), Kennett and Srinivasan (1983), Bolli and Saunders (1985), Chaisson and Leckie (1993), Loeblich and Tappan (1994), Weiner et al. (2015), Wade et al. (2018), and Bylinskaya (2004).

In this study, we differentiated *Neogloboquadrina pachyderma* from *Neogloboquadrina incompta* because they are regarded as two distinct species based on biogeographic, ecological, and genetic differentiation (Brummer and Kroon, 1988; Darling et al., 2006). Specifically, we assigned the right-coiling type to *Neogloboquadrina incompta* and the left-coiling type to *Neogloboquadrina pachyderma* (Darling et al., 2006). Both *Neogloboquadrina pachyderma* and *Neogloboquadrina incompta* were separated from *Neogloboquadrina dutertrei* following Lam and Leckie (2020). The species name *Neogloboquadrina dutertrei* was given to individuals possessing 5–6 chambers and with an open and deep umbilical area. Conversely, *Neogloboquadrina pachyderma* and *Neogloboquadrina incompta* show 4–4.5 chambers in the final whorl, a subquadrate to quadrate outline, and a less open and deep umbilicus. Furthermore, we identified as *Neogloboquadrina acostaensis* all the specimens showing 5–5.5 chambers in the final whorl with straight sutures on both umbilical and spiral sides and with a wide apertural

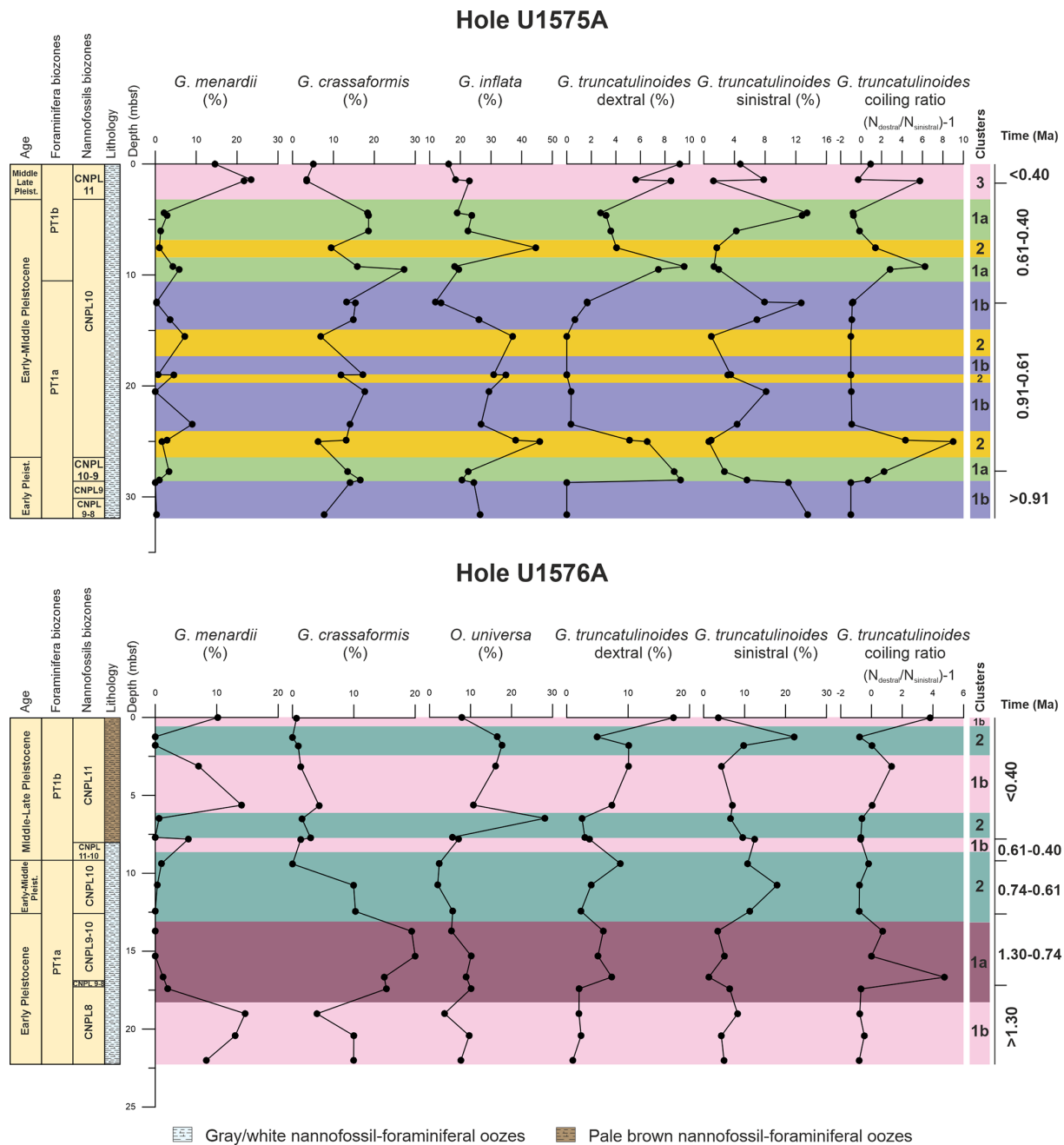


Figure 3. Relative abundances (%) plotted against depth (m b.s.f.) of the planktonic foraminiferal species which define the clusters in Holes U1575A and U1576A. The figure also shows the ratio between right- and left-coiling tests of *Globorotalia truncatulinoides*. Foraminifera and calcareous nannofossil biozonations and the lithological units are also indicated. Numerical age intervals are expressed in Ma. Clusters for Hole U1575A are indicated as follows. 1a: expanded SACW intrusion; 1b: limited SACW intrusion; 2: normal BOC conditions; 3: Agulhas Leakage. Clusters for Hole U1576A are indicated as follows. 1a: expanded SACW intrusion; 1b: Agulhas Leakage; 2: nutrient filaments within the BOC.

rim/plate (Lam and Leckie, 2020). This species differs from *Neogloboquadrina dutertrei* by showing a narrower umbilicus with the rim/plate covering most of the umbilical area (Kennett and Srinivasan, 1983).

2.2.2 Calcareous nannofossils

The identification of calcareous nannofossils was based on *The Handbook of Cenozoic Calcareous Nannoplankton* Volumes 1–4 (Aubry, 1984, 1988, 1989, 1990), Perch-Nielsen (1985a, b), Young (1998), Wade and Bown (2006), Bown and

Dunkley Jones (2012), and Nannotax3 (Young and Bown, 2017).

The taxonomy of *Reticulofenestra asanoi* follows Maiorano and Marino (2004). Specifically, circular to subcircular specimens without slits and larger than 6 μm were identified as *Reticulofenestra asanoi*. Conversely, subcircular morphotypes $\geq 5 \mu\text{m}$, with (few) slits and a wider central area, were indicated as *Reticulofenestra* sp. All elliptical reticulofenestrids larger than 5 μm and with a central opening were classified as *Reticulofenestra pseudoumbilicus* (see Young, 1990).

Gephyrocapsa placoliths were differentiated based on the size ranges defined by Raffi (2002): small (< 4 μm), medium (4–5.5 μm), and large (> 5.5 μm). The differentiation between *Calcidiscus tropicus* and *Calcidiscus macintyreii* follows Young (1998): individuals greater than 10 μm were assigned to *Calcidiscus macintyreii*, and those smaller than 10 μm were assigned to *Calcidiscus tropicus*.

2.3 Sample preservation

2.3.1 Planktonic foraminifera

The preservation of planktonic foraminifera was rated as follows (see Tables S1–S2): VG, very good (shells exhibiting an absence of recrystallization and overgrowth, with all specimens recognizable at the species level); G, good (tests showing only minor signs of recrystallization and overgrowth, with almost all individuals identified at species level); M, moderate (common recrystallization and overgrowth observed on the foraminiferal shells, with most individuals recognizable at the species level); and P, poor (shells exhibiting substantial recrystallization and overgrowth, with identification at the species level often very difficult).

2.3.2 Calcareous nannofossils

Preservation for calcareous nannofossils was evaluated as follows (see Tables S1–S2): VG, very good (specimens do not exhibit dissolution and overgrowth, with all diagnostic features preserved); G, good (specimens show minor dissolution and overgrowth, with morphological characteristics slightly altered); M, moderate (individuals exhibit moderate dissolution, overgrowth, and etching, with not all specimens recognizable at the species level); and P, poor (specimens show a high grade of dissolution, overgrowth, and etching, with morphological features highly affected and most of the individuals not being identifiable at the species level).

2.4 Biostratigraphy

Biostratigraphic events for planktonic foraminifera were obtained from Gradstein et al. (2020), whereas age assignments for calcareous nannofossils were based on Wei (1993), Raffi (2002), and Gradstein et al. (2020).

The biozonation for calcareous nannofossils follows Backman et al. (2012), while planktonic foraminifera biostratigraphic zones are according to Wade et al. (2011). Local bioevents were defined using base (B) and top (T), as well as the base common (Bc) and top common (Tc) occurrences of marker taxa (see Tables S1–S2, 1, and 2). We calculated a depth error value for each biostratigraphic event (Tables 1 and 2), which represents the uncertainty of the depth at which a specific biohorizon (species' base/top) occurs within the sequence. Specifically, the maximum potential depth error for the planktonic foraminifera and calcareous nannofossil datums is expressed as the sample spacing between the sample in which the specific bioevent was placed and the stratigraphically next sample (for the top occurrence) or previous sample (for the base occurrence).

2.5 Statistical analyses and ordination

At least 300 individuals per sample were picked and identified for the paleoecological investigation of the planktonic foraminifera assemblages. The relative abundance of the recognized species was expressed as a percentage of the total count of individuals in each sample (Tables S3–S4).

Statistical and ordination analyses in this study include the similarity percentage (SIMPER) analysis, cluster analysis (unweighted pair group method with arithmetic mean; UP-GMA), and principal component analysis (PCA), which were executed using the software PAST (version 4.09) (Hammer et al., 2001). Planktonic foraminifera relative abundances were arcsine root transformed (e.g., Sokal and Rohlf, 1995) before the multivariate analyses to ensure a normal distribution of the data values (e.g., Auer et al., 2019; Del Gaudio et al., 2023). Using the Bray–Curtis similarity index, the UP-GMA was computed to define the clusters (Tables S3–S4 and Fig. 4). Moreover, the bootstrapping ($N = 1000$) function was used to test the stability of the clusters. The contribution of the species to the clusters was evaluated using the SIMPER analysis (using Bray–Curtis similarity). The clustering was performed, including and excluding biostratigraphic markers from the dataset, to assess their influence on the distributions of the clusters.

PCA was also performed to detect the principal environmental components (variables) controlling the planktonic foraminifera assemblages and to assess the results obtained from the cluster analysis (Figs. S1–S2). Taxa with an average percentage lower than 2 % were excluded from statistical and ordination analyses. Species belonging to the *Trilobatus* plexus were grouped together, as they genetically represent a single biological taxon (Hemleben et al., 1987; André et al., 2013). Specimens belonging to the tropical/subtropical morphotypes *Globigerinoides ruber* sensu stricto (s.s) and sensu lato (s.l.) (see Wang, 2000; Jayan et al., 2021; Del Gaudio et al., 2023) were also lumped together as *Globigerinoides ruber* (white). This is because their abundances are too low to

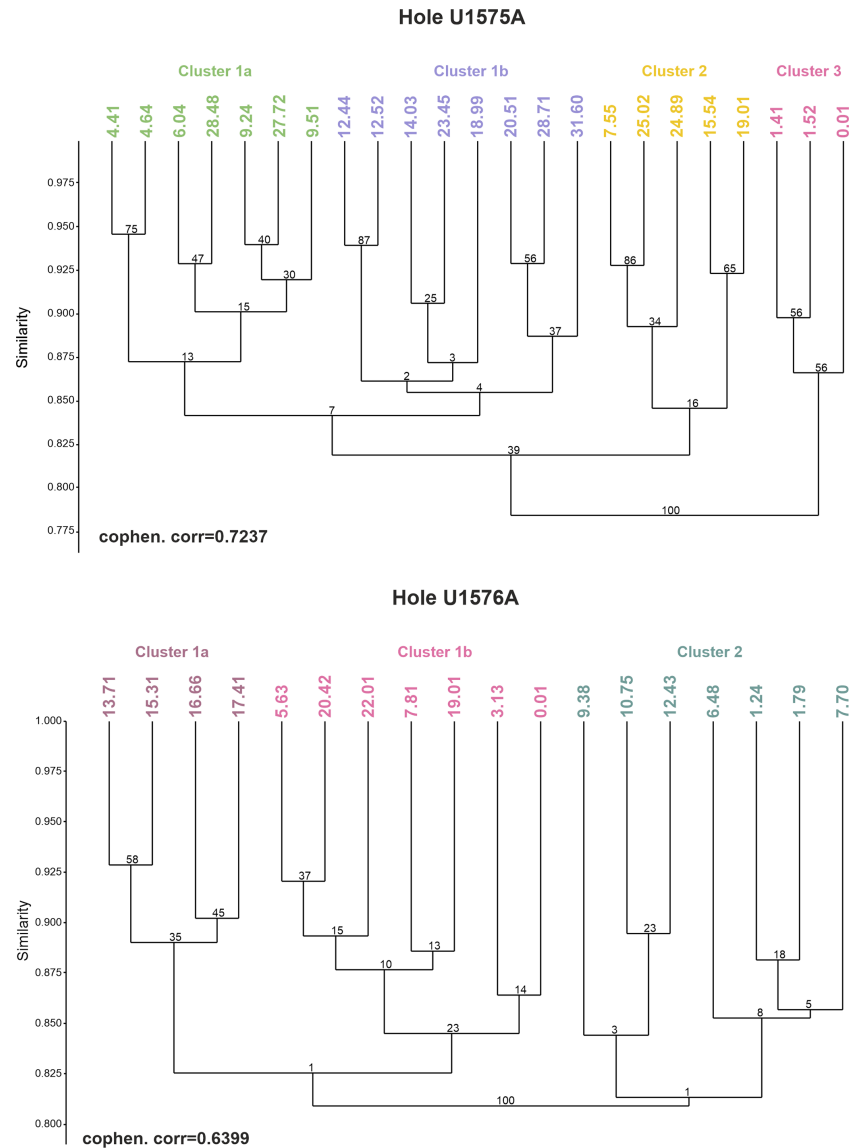


Figure 4. UPGMA dendrograms of cluster analysis for Holes U1575A and U1576A.

possibly infer any valuable variations in the paleoecological conditions at middle latitudes.

The *Globorotalia truncatulinoides* coiling ratio was computed, as it reflects paleoenvironmental variations, such as the thermal structure of the upper water column (e.g., Thiede, 1971; Pickard and Emery, 1991). Specifically, the ratio was obtained using the total test count of the left and right morphotypes, normalized to 0 (Tables S3–S4).

The Agulhas Leakage represents an inflow of warm and saline waters from the Indian Ocean to the southeastern Atlantic Ocean (Fine et al., 1988; Petrick et al., 2015; Friesenhagen, 2022). To evaluate the capability of the possible water exchanges between the Indian Ocean and the Atlantic Ocean (Tables S3–S4 and Fig. 5), we calculated the Agulhas Leakage efficiency (ALE) index (Caley et al., 2014). The index is

expressed as follows:

$$\text{ALE}(\%) = (\text{IOTG}/(\text{IOTG} + \text{SOG})) \cdot 100. \quad (1)$$

The Indian Ocean Tropical Group (IOTG) represents the species which strictly characterize the Agulhas water masses (e.g., *Globorotalia menardii*, *Trilobatus* spp.), while the Southern Ocean Group (SOG) is composed of taxa which thrive in cold, transitional, and subpolar water masses (e.g., *Globigerina bulloides*, *Globoconella inflata*, *Neogloboquadrina pachyderma*). Both IOTG and SOG are defined as the sum of the total count of each species belonging to the groups. We excluded all taxa with low abundances (< 0.5 %) or that are not indicative of either of the two groups, following Caley et al. (2014).

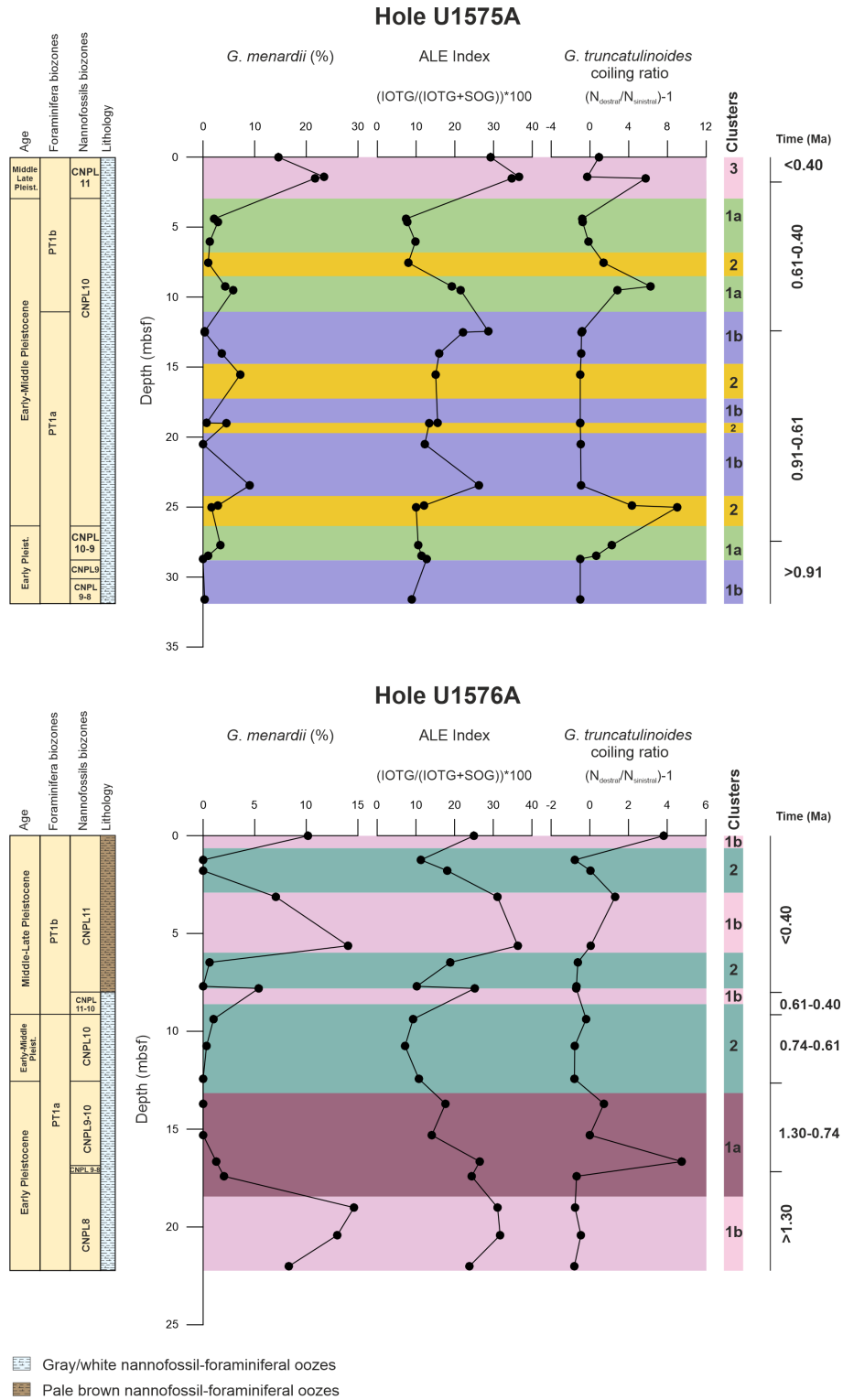


Figure 5. The graphs represent relative abundances (%) of *Globorotalia menardii*, the ALE index, and the *Globorotalia truncatulinoides* dextral and sinistral coiling ratio. Foraminifera and calcareous nannofossil biozonations and the lithological units are also indicated. Numerical age intervals are expressed in Ma. Clusters for Hole U1575A are indicated as follows. 1a: expanded SACW intrusion; 1b: limited SACW intrusion; 2: normal BOC conditions; 3: Agulhas Leakage. Clusters for Hole U1576A are indicated as follows. 1a: expanded SACW intrusion; 1b: Agulhas Leakage; 2: nutrient filaments within the BOC.

3 Results

3.1 Integrated biostratigraphy

Integrated calcareous nannofossil and planktonic foraminiferal biostratigraphic investigations allowed the determination of 11 bioevents for Hole U1575A and 9 bioevents for Hole U1576A.

Detected bioevents, taxa, and semi-quantitative abundance data for calcareous nannofossils and planktonic foraminifera are summarized in Tables 1–2 and S1–S2. Biostratigraphic events are examined in detail in the Discussion.

3.2 Preservation and reworking

The preservation of planktonic foraminifera and calcareous nannofossils is indicated in Tables S1–S2. Planktonic foraminiferal tests were generally very well to well preserved in Holes U1575A and U1576A. However, several samples in Hole U1575A (18.98–20.52 m b.s.f.) showed good to moderate preservation, with specimens slightly affected by overgrowth and etching.

The preservation of calcareous nannofossils in Hole U1576A varies from good to very good, with most of the individuals exhibiting minor evidence of dissolution/overgrowth and displaying all their diagnostic features in a perfectly recognizable way. Sediments in Hole U1575A contained well preserved specimens, with only two samples (between 18.98 and 20.52 m b.s.f.) moderately affected by dissolution/overgrowth.

Reworking of planktonic foraminifera and calcareous nannofossils was observed within the studied stratigraphic sequence at both sites (see Tables S1–S2). Its evaluation relied on the biostratigraphic distribution of the identified species and on changes in the color and preservational state of the reworked forms compared to the in situ assemblage. Planktonic foraminiferal Miocene to Early Pleistocene reworked taxa include *Globoconella miozea*, *Globoconella punctulata*, and *Globigerinoides bollii*. In Hole U1575A, the reworking mainly affected sediments between 18.27 and 19.02 m b.s.f., in which a high number of reworked species were detected (see Tables S1–S2). Calcareous nannofossils instead showed Cretaceous and Paleogene to Miocene reworked forms such as *Bomolithus* spp., *Ericsonia* spp., *Helicosphaera vedderi*, and *Discoaster druggii*.

3.3 Planktonic foraminiferal assemblage distribution

An average of 304 (min = 283; max = 327) and 308 (min = 297; max = 346) specimens per sample were counted and identified for the assemblage study in Holes U1575A and U1576A, respectively. At both locations, the microfossil assemblages were dominated by planktonic foraminifera, whereas individuals of benthic foraminifera and ostracod shells were only sporadically observed. Planktonic

foraminiferal relative abundance data and statistical results are shown in Tables S3–S4 and Figs. 3–5.

3.3.1 Cluster analyses and ordination in Hole U1575A

UPGMA cluster analysis classified the samples into three main clusters (Table S3 and Fig. 4). The differentiation between the clusters was attained at a cut-off distance of ~0.81. The cophenetic correlation coefficient obtained from the application of UPGMA clustering is 0.7237. Additionally, cluster 1 can be separated into two subclusters (1a and 1b), with a cut-off score of ~0.83.

SIMPER analysis (%) was used to identify which species mostly contributed to the cluster separation (Table S3 and Fig. 3). The separation of clusters 1 and 2 largely relies on *Globoconella inflata* (contribution > 19 %) and *Globorotalia truncatulinoides* sinistral and dextral forms, which account for 14.76 % and 13.02 % of the dissimilarity, respectively. Other species include *Globorotalia crassaformis* (10.5 %), *Globorotalia menardii* (9.59 %), *Orbulina universa* (6.21 %), and *Globigerina bulloides* (5.7 %).

Clusters 1 and 3 are distinguished based on *Globorotalia menardii* (27.05 %), *Globorotalia crassaformis* (17.05 %), and *Globorotalia truncatulinoides* dextral (12.10 %) and sinistral (8.33 %). Minor contributors include *Neogloboquadrina pachyderma* (7.30 %), *Orbulina universa* (6.44 %), and *Neogloboquadrina incompta* (5.85 %). The abundance of *Globorotalia menardii* (22.17 %) and *Globoconella inflata* (18.18 %) is the primary distinction between clusters 2 and 3. Other species include *Globorotalia truncatulinoides* dextral (11.44 %), *Globorotalia crassaformis* (8.59 %), *Neogloboquadrina incompta* (7.83 %), and *Globorotalia truncatulinoides* sinistral (7.69 %). The difference between subclusters 1a and 1b primarily depends on *Globorotalia truncatulinoides* dextral (21.48 %), *Globorotalia menardii* (13.06 %), and *Globorotalia truncatulinoides* sinistral (12.39 %). Minor contributions derive from *Globoconella inflata* (9.48 %), *Globigerinoides ruber* (7.48 %), and *Globorotalia crassaformis* (7.19 %).

The average abundance (%) of planktonic foraminiferal taxa for each cluster/subcluster was also calculated and shown in Table S3. Moreover, the abundances of the dominant species are plotted in Fig. 3. Planktonic foraminifera assemblage of subcluster 1a is dominated by *Globoconella inflata* (20.83 %) and *Globorotalia crassaformis* (18.37 %). Other common species include *Neogloboquadrina incompta* (14.91 %), *Globigerina bulloides* (7.08 %), and *Globorotalia truncatulinoides* dextral (6.37 %) and sinistral (6.01 %). Foraminiferal association based on subcluster 1b showed a higher abundance of *Globoconella inflata* (23.68 %) and *Globorotalia truncatulinoides* sinistral (8.52 %) and lower values of *Globorotalia crassaformis* (14.26 %) and *Globorotalia truncatulinoides* dextral (0.58 %) compared to subcluster 1a. Furthermore, the assemblage also comprises *Neogloboquadrina incompta* (11.28 %) and *Globigerina bul-*

loides (8.02 %). The most representative taxa of cluster 2 are *Globoconella inflata* (with the highest values of 40.08 %), *Neogloboquadrina incompta* (15.52 %), *Globorotalia crassaformis* (9.50 %), and *Globigerina bulloides* (7.18 %).

The foraminiferal assemblage of cluster 3 shows consistently high abundances of *Globorotalia menardii* (19.91 %) and *Globoconella inflata* (19.19 %), with low abundances of *Globorotalia crassaformis* (3.99 %). This cluster is also characterized by an increase in abundance of the tropical/subtropical taxa, such as *Trilobatus* spp. (1.68 %) and *Globoturborotalita rubescens* (1.69 %).

PCA analysis was performed to assess which species contribute the most to each principal component (Fig. S1). PCA results indicate that three variables account for 76 % of the variance (PC1 = 37.38, PC2 = 22.11, and PC3 = 16.44 %). *Globorotalia menardii* and *Globorotalia truncatulinoides* dextral mainly dominate the component PC1, whereas negative loadings of PC1 largely depend on *Globorotalia crassaformis* and *Globorotalia truncatulinoides* sinistral. The second principal component (PC2) is largely positively correlated to *Globorotalia crassaformis* and *Globorotalia truncatulinoides* sinistral and dextral, while the negative loadings are heavily related to *Globoconella inflata*. Principal component three (PC3) is positively associated with high scores of *Globorotalia crassaformis* and *Globorotalia truncatulinoides* dextral, whereas *Globorotalia menardii* and *Globorotalia truncatulinoides* sinistral dominate the negative loadings.

The ALE index, calculated on our dataset (Table S3), showed high percentages (33.50 %) in cluster 3, whereas lower values were observed for the remaining clusters (cluster 1a = 12.52 %, cluster 1b = 17.79 %, and cluster 2 = 11.69 %). The ratio between dextral and sinistral variants of *Globorotalia truncatulinoides* is shown in Fig. 3 and Table S3. The highest positive ratios were recorded in clusters 2 (average 2.55) and 3 (2.13), whereas the most negative values were obtained for cluster 1b (−0.93). Cluster 1a also shows positive values but far lower than those recorded for clusters 2 and 3. No correspondence was observed between the trend in abundance of *Globorotalia menardii* and the variation in the *Globorotalia truncatulinoides* ratio plotted against depth (see Fig. 5).

3.3.2 Cluster analyses and ordination in Hole U1576A

Two main clusters were obtained in Hole U1576A using the UPGMA hierarchical clustering algorithm. Cluster 1 was separated into subclusters 1a and 1b (Table S4 and Fig. 4). The separation between the two main clusters was obtained with a cut-off distance of ~ 0.80.

Based on SIMPER analysis (Table S4), the difference between clusters 1 and 2 relies on *Globorotalia menardii* (contribution of 18.99 %), *Globorotalia crassaformis* (17.19 %), *Orbulina universa* (12.51 %), and *Globorotalia truncatulinoides* sinistral (12.27 %). Other species include *Globoro-*

talia truncatulinoides dextral (8.21 %) and *Neogloboquadrina incompta* (8.16 %). Subclusters 1a and 1b are largely distinguished based on *Globorotalia menardii* (25.77 %) and *Globorotalia crassaformis* (23.37 %). Minor contributors include *Globorotalia truncatulinoides* dextral (9.87 %), *Globorotalia truncatulinoides* sinistral (7.35 %), and *Orbulina universa* (5.77 %).

Average relative abundance data indicate that the most indicative species for subcluster 1a are *Globoconella crassaformis* (17.43 %) and *Globoconella inflata* (17.18 %). Other species include *Globigerinoides ruber* (7.01 %), *Globigerinita glutinata* (6.12 %), and *Globigerina bulloides* (5.80 %). The foraminiferal assemblage of subcluster 1b shows a high abundance of *Globoconella inflata* (17.49 %), *Globorotalia menardii* (10.36 %), and *Neogloboquadrina incompta* (9.90 %). Other species include *Globigerina bulloides* (7.95 %), *Globorotalia truncatulinoides* dextral (6.26 %) and sinistral (6.43 %), *Globigerinita glutinata* (5.05 %), and *Globorotalia crassaformis* (4.52 %). Cluster 2 is dominated by *Globoconella inflata* (20.79 %), *Globorotalia truncatulinoides* sinistral (12.56 %), *Neogloboquadrina incompta* (13.16 %), and *Orbulina universa* (11.12 %), with minor contributions from *Globigerina bulloides* (9.05 %) and *Globigerinoides ruber* (5.05 %).

PCA analysis (Fig. S2) highlighted that three variables are responsible for 80.27 % of the variance (PC1 = 31.90, PC2 = 28.71, and PC3 = 19.66 %). The first principal component (PC1) mainly depends on *Globorotalia crassaformis*. Conversely, PC1 is negatively correlated with *Globorotalia menardii* and *Globorotalia truncatulinoides* dextral and sinistral. *Globorotalia menardii* positively dominates the PC2, while *Globorotalia truncatulinoides* sinistral, *Neogloboquadrina incompta*, and *Globoconella inflata* are negatively correlated to PC2. PC3 positive loadings mainly rely on *Neogloboquadrina incompta* and *Globorotalia truncatulinoides* sinistral. In contrast, *Orbulina universa* dominates the negative loading, with a minor contribution from *Globorotalia menardii* and the right-coiling type of *Globorotalia truncatulinoides*.

The ALE index for Hole U1576A exhibits the highest percentage (average 29.19 %) in cluster 1b, whereas clusters 1a and 2 show lower values (20.67 % and 12.24 %, respectively; see Table S4).

The *Globorotalia truncatulinoides* dextral / sinistral ratio (see Table S4 and Fig. 3) shows positive values for cluster 1a (average 1.19) and 1b (0.35). Cluster 2 exhibits negative values of the ratio (−0.545). As also previously observed for Hole U1575A, the relative abundances (against depth) of *Globorotalia menardii* do not follow the changes in abundance of the right and left variants of *Globorotalia truncatulinoides* (see Fig. 5).

4 Discussion

4.1 Integrated biostratigraphy

Integrated calcareous nannofossils and planktonic foraminifera biostratigraphy enabled us to provide a well-defined stratigraphic record for Holes U1575A and U1576A and to improve the biostratigraphic resolution obtained during the IODP shipboard investigations (Sager et al., 2023). Sediment samples used for this study were not collected within the cores between biostratigraphic horizons, leading to an uncertainty in the placement of the biostratigraphic events. To evaluate the degree of this uncertainty for the bioevents, we calculated the maximum potential depth error (see Sect. 2.4 in Materials and methods) rather than the mid-point depth approach (commonly used in IODP data reporting), where a bioevent is placed as a mid-point between the sample in which a taxon is first (or last) recorded and the sample stratigraphically below (or above) within which the taxon is not present. We deliberately chose this approach because using the mid-point depths obscures critical information on the potential sampling bias in depth direction (top and base occurrences can logically only have an error up and downward section, respectively). Thus, the use of the maximum potential depth error has the benefit that its degree of freedom is, per definition, unidirectional for each event. Moreover, we can add additional and highly valuable information and details to the generated age–depth model.

4.1.1 Hole U1575A

The studied stratigraphic sequence spans from the Late Pliocene (Piacenzian) to the Quaternary, according to planktonic foraminiferal and calcareous nannofossil datums (Tables 1 and S1). The oldest possible age interval recorded at Hole U1575A (Sample U1575A-5R-7W, 0–2 cm; 46.89 m b.s.f.) is between 3.13 and 3.24 Ma, based on the top (T) occurrence of *Dentoglobigerina altispira* (Wade et al., 2011; Gradstein et al., 2020) and the base (B) of the planktonic taxon *Globoconella inflata* (Gradstein et al., 2020). The concomitant presence of *Dentoglobigerina altispira* and *Globoconella inflata* allowed the assignment of the sample to planktonic foraminifera zones PL3–PL4 (Wade et al., 2011) and calcareous nannofossil zone CNPL4 (Backman et al., 2012). Sediments between 46.89 and 44.20 m b.s.f. were dated younger than 3.13 and older than 1.98 Ma (PL4–PL6 and CNPL4–CNPL6 zones), based on the absence of *Dentoglobigerina altispira* and *Globorotalia truncatulinoides* (B 1.93 Ma; Gradstein et al., 2020). A possible hiatus can be placed between 44.20 and 46.89 m b.s.f., as an abrupt change in the sedimentation rate can be observed within this interval. However, the presence of the hiatus cannot be confirmed with certainty due to the lack of available samples between sections 4W and 7W in Core 5H.

The top occurrence of *Neogloboquadrina acostaensis* (1.58 Ma; Gradstein et al., 2020) occurred at 32.59 m b.s.f. (Sample U1575A-4R-3W, 88–90 cm). The sediment between the basal occurrence of *Globorotalia truncatulinoides* and the top occurrence of *Neogloboquadrina acostaensis* encompasses the biozones PL6–PT1a and CNPL6–CNPL8. Among calcareous nannofossils, *Calcidiscus macintyreii* (T 1.60 Ma; Gradstein et al., 2020) and *Gephyrocapsa* spp. > 5.5 µm (B 1.59 Ma; Gradstein et al., 2020) were also detected in the abovementioned depth interval. However, *Gephyrocapsa* spp. > 5.5 µm was present only in two samples (U1575A-4R-2W, 138–140 cm, and U1575A-4R-3W, 88–90 cm; 31.59–32.61 m b.s.f.), whereas the stratigraphic appearance of *Calcidiscus macintyreii* was rare and scattered, making the placement of the bioevent extremely difficult. Furthermore, its last occurrence is regarded as poorly accurate due to ambiguous taxonomic identifications (Raffi et al., 1995, 2006). For all the reasons discussed above, the use of *Neogloboquadrina acostaensis* as a biostratigraphic marker is preferred here.

The top occurrence of *Helicosphaera sellii* (1.24 Ma; Gradstein et al., 2020) is located at 31.59 m b.s.f. (Sample U1574A-4R-2W, 138–140 cm). This bioevent is well defined (Raffi et al., 2006) and is regarded as isochronous in the equatorial and mid-latitude sectors of the Atlantic Ocean (Gradstein et al., 2020). The stratigraphic interval between the top occurrences of *Neogloboquadrina acostaensis* and *Helicosphaera sellii* falls within zones PT1a and CNPL8–CNPL9.

Two important biostratigraphic horizons were detected between 28.49 and 26.51 m b.s.f.: the base common (Bc) and the top common (Tc) occurrences of *Reticulofenestra asanoi* (1.14 and 0.91 Ma, respectively; Gradstein et al., 2020) were used to restrict the depth interval to zones PT1a and CNPL9–CNPL10. The stratigraphic distribution of *Reticulofenestra asanoi* is constrained to the Early–Late Pleistocene (Sato et al., 1991; Wei, 1993; Raffi, 2002; Maiorano and Marino, 2004), with the first and last common occurrences of the species regarded as more reliable than its absolute first and last appearances (Maiorano and Marino, 2004).

Sediments above the top common *Reticulofenestra asanoi* and the basal occurrence of *Globorotalia hessi* (0.74 Ma; Gradstein et al., 2020) fall within zones PT1a and CNPL10. Calcareous nannofossil assemblages in this depth interval (19.02–26.51 m b.s.f.) also contain a few specimens of *Reticulofenestra asanoi* and *Reticulofenestra* sp. However, while the occurrences of *Reticulofenestra asanoi* are discontinuous above its Tc (Maiorano and Marino, 2004), the placement of the last appearance of *Reticulofenestra* sp. was found to be inconsistent in previously studied Atlantic sections (Maiorano and Marino, 2004). Thus, the use of B *Globorotalia hessi* as a bioevent is favored here.

Globorotalia tosaensis shows a fairly continuous stratigraphic distribution in Hole U1575A (between 44.20 and 12.43 m b.s.f.), and its top occurrence (0.61 Ma; Gradstein et al., 2020) was used to determine the base of subzone

Table 1. Calcareous nannofossil and planktonic foraminifera bioevents detected in Hole U1575A. B: base; T: top; Bc: base common occurrence; Tc: top common occurrence.

Bioevent	Age (Ma)	Sample ID	Depth (m b.s.f.)	Depth error (m b.s.f.)	Reference
B <i>G. calida</i>	0.22	1R-1W, 0–2	0.02	1.38	Gradstein et al. (2020)
B <i>E. huxleyi</i>	0.29	1R-1W, 140–142	1.42	0.09	Gradstein et al. (2020)
B <i>G. flexuosa</i>	0.40	1R-2W, 0–2	1.53	0.58	Gradstein et al. (2020)
T <i>P. lacunosa</i>	0.43	1R-3W, 138–140	4.40	1.26	Gradstein et al. (2020)
T <i>G. tosaensis</i>	0.61	2R-2W, 143–145	12.43	2.91	Gradstein et al. (2020)
B <i>G. hessi</i>	0.74	3R-1W, 0–2	19.02	1.48	Gradstein et al. (2020)
T common <i>R. asanoi</i>	0.91	3R-6W, 0–2	26.51	1.48	Gradstein et al. (2020)
B common <i>R. asanoi</i>	1.14	3R-7W, 65–67	28.49	0.23	Gradstein et al. (2020)
T <i>H. sellii</i>	1.24	4R-2W, 138–140	31.59	2.87	Gradstein et al. (2020)
T <i>N. acostaensis</i>	1.58	4R-3W, 88–90	32.59	0.98	Gradstein et al. (2020)
B <i>G. truncatulinoides</i>	1.93	5R-4W, 137–139	44.20	2.69	Gradstein et al. (2020)

PT1b (Wade et al., 2011), which, in turn, corresponds to zone CNPL10 of Backman et al. (2012). The concomitant extinctions of *Globorotalia ronda* at ~0.6 Ma (Bylinskaya, 2004; Aze et al., 2011) in the stratigraphic sequence further support the validity of the discussed bioevent. The top occurrence of *Pseudoemiliania lacunosa* (0.43 Ma; Gradstein et al., 2020) and the basal occurrence of *Globorotalia flexuosa* (0.40 Ma; Gradstein et al., 2020) occurred at 4.40 and 1.53 m b.s.f., allowing us to assign the sediments to zones PT1b and CNPL10–CNPL11.

The topmost biostratigraphic events detected in Hole U1575A were the base of *Emiliania huxleyi* (0.29 Ma; Gradstein et al., 2020) and *Globigerinella calida* (0.22 Ma; Gradstein et al., 2020), detected at 1.42 and 0.02 m b.s.f., respectively. The previously mentioned bioevents constrain the stratigraphic interval to zones PT1b and CNPL11.

4.1.2 Hole U1576A

The analyzed sediment interval in Hole U1576A comprises Early to Late Quaternary deposits (Tables 2 and S2).

The bottommost part of the stratigraphic sequence (28.58 m b.s.f.) is dated older than 1.98 Ma but younger than 3.24 Ma, based on the top occurrence of *Globigerinoides extremus* (Gradstein et al., 2020) and the basal appearance of *Globoconella inflata* (B 3.24 Ma; Gradstein et al., 2020). The assigned biozones for the interval were PL6–PL3 and CNPL6–CNPL4 for planktonic foraminifera and calcareous nannofossils, respectively.

The top occurrence of *Discoaster brouweri* (1.93 Ma; Gradstein et al., 2020) was recorded at 27.60 m b.s.f., constraining the age of the sediments to zones PL6 and CNPL6. The following biohorizon is represented by the top occurrence of *Neogloboquadrina acostaensis* (1.58 Ma; Gradstein et al., 2020), which constrains the sediment between 27.60 and 23.40 m b.s.f. to zones PL6–PT1a and CNPL6–CNPL8. Similarly to Hole U1575A, the occurrence of *Calcidiscus*

macintyreii (T 1.60 Ma; Gradstein et al., 2020) was not considered at this site. The last appearance datum of *Globigerinoides obliquus* (T 1.30 Ma; Gradstein et al., 2020) was detected at 17.40 m b.s.f., constraining the interval below to zones PT1a and CNPL8.

The stratigraphic interval observed at Site U1575, characterized by a distinct increase in the abundance of *Reticulofenestra asanoi*, was not recorded at Hole U1576A. However, it was possible to use the first absolute occurrence of *Reticulofenestra asanoi* (B 1.17 Ma; Raffi, 2002) to assign the sediments between this biohorizon and T *Globigerinoides obliquus* to zones PT1a and CNPL8–CNPL9. Although not as distinct as the Bc *Reticulofenestra asanoi* event (1.14 Ma; Gradstein et al., 2020), the first appearance datum of *Reticulofenestra asanoi* is still regarded as a useful biohorizon in Pleistocene deposits (Takayama and Sato, 1987; Wei, 1993; Raffi, 2002).

The base of *Globorotalia hessi* (0.74 Ma; Gradstein et al., 2020) was observed in Sample U1576-2R-4W, 20–22 cm (12.44 m b.s.f.). This bioevent, together with the B of *Reticulofenestra asanoi*, constrained the age of the sediments to PT1a and CNPL9–CNPL10. The top of the planktonic foraminiferal subzone PT1a was defined at Hole U1576A by the top occurrence of *Globorotalia tosaensis* (0.61 Ma; Wade et al., 2011). The sediments between B *Globorotalia hessi* and T *Globorotalia tosaensis* were assigned to zones PT1a and CNPL10.

The youngest biostratigraphic events observed at this site were the base of *Globorotalia flexuosa* (0.40 Ma; Gradstein et al., 2020) and *Globigerinella calida* (0.22 Ma; Gradstein et al., 2020), occurring at 7.82 and 3.14 m b.s.f., respectively. These bioevents allowed us to assign sediments to zones PT1b and CNPL11.

Table 2. Calcareous nannofossil and planktonic foraminifera bioevents detected in Hole U1576A. B: base; T: top; Bc: base common occurrence; Tc: top common occurrence.

Bioevent	Age (Ma)	Sample ID	Depth (m b.s.f.)	Depth error (m b.s.f.)	Reference
B <i>G. calida</i>	0.22	1R-3W, 60–62	3.14	2.48	Gradstein et al. (2020)
B <i>G. flexuosa</i>	0.40	2R-1W, 0–2	7.82	1.55	Gradstein et al. (2020)
T <i>G. tosaensis</i>	0.61	2R-2W, 10–12	9.37	1.55	Gradstein et al. (2020)
B <i>G. hessi</i>	0.74	2R-4W, 20–22	12.44	0.08	Gradstein et al. (2020)
B <i>R. asanoi</i>	1.17	2R-7W, 0–2	16.67	0.73	Wei (1993), Raffi (2002)
T <i>G. obliquus</i>	1.30	3R-1W, 0–2	17.40	0.73	Gradstein et al. (2020)
T <i>N. acostaensis</i>	1.58	3R-5W, 0–2	23.40	1.38	Gradstein et al. (2020)
T <i>D. brouweri</i>	1.93	4R-1W, 60–61	27.60	0.58	Gradstein et al. (2020)
T <i>G. extremus</i>	1.98	4R-2W, 10–12	28.58	0.97	Gradstein et al. (2020)

4.2 Paleooceanographic conditions in the northern Benguela system inferred from the planktonic foraminiferal assemblages

Variations in the planktonic foraminiferal assemblages during the Quaternary can be interpreted as indicative of changes in the water mass dynamics within the northern Benguela system. In this respect, quantitative analyses performed on the foraminiferal communities (UPGMA and PCA) revealed different paleooceanographic settings in Holes U1575A and U1576A, with an average time resolution for the sampling between 50 (Hole U1575A) and 70 kyr (U1576A). Specifically, UPGMA defined several clusters representing distinct planktonic assemblages, reflecting different environmental conditions. Furthermore, the use of PCA allowed us to define which paleoenvironmental variables affect the planktonic assemblages.

4.2.1 Hole U1575A

Three major clusters were defined for Hole U1575A, reflective of the existence of three main paleooceanographic conditions, as follows (Figs. 3–5 and 6; Table S3):

- *Normal BOC conditions (cluster 2)*. This cluster is dominated by *Globoconella inflata*, representing 40 % of the total assemblage. *Neogloboquadrina incompta* and *Globigerina bulloides* also show common abundances. The three abovementioned species are commonly found within the BOC, which represents the relatively oligotrophic and less cold (17–22 °C; Rouault and Tomety, 2022) offshore component of the Benguela current system (Giraudeau, 1993; Little et al., 1997; Ufkes and Kroon, 2012). Conversely, species like *Neogloboquadrina pachyderma* and *Turborotalita quinqueloba* (constantly exhibiting low abundances in our record) thrive in the more nutrient-rich and cooler (15–17 °C; Rouault and Tomety, 2022) surface waters of the BCC and constitute the typical upwelling fauna (Giraudeau, 1993; Little et al., 1997). Specifically, the abundances

of *Globoconella inflata*, *Neogloboquadrina incompta*, and *Globigerina bulloides* were previously found to increase offshore (away from the coast), based on several retrieved cores (Giraudeau, 1993). *Globorotalia crassaformis* is typically associated with warm and low-oxygenated subsurface waters (SACW) situated in the Angola Basin, north of the ABF (van Leeuwen, 1989; Oberhänsli et al., 1992; Ufkes and Kroon, 2012). Thus, the variation in abundance of *Globorotalia crassaformis* reflects a north–south shifting of the thermal ABF (Ufkes and Kroon, 2012), with higher values indicating southward fluctuations of the ABF and the expansion of the Angola warm waters within the northern Benguela region (Shannon et al., 1986; Monteiro and van der Plas, 2006). In cluster 2, this taxon exhibits low abundances, accounting for only 9.50 % of the assemblage. Thus, we interpreted the foraminiferal association of cluster 2 as indicative of what we described as normal Benguela conditions. This definition refers to a system where the ABF is located north of the Benguela region so that the BOC waters are not perturbed by the southward intrusions of the SACW (Fig. 6). This is further corroborated by the high amount of *Globorotalia inflata*, which thrives in the cooler water of the BOC and shows an opposite trend in abundance compared to *Globorotalia crassaformis*. The right- and sinistral-coiling types of *Globorotalia truncatulinoides* show distinct environmental conditions, as underlined by several studies (e.g., Herman, 1972; Lohmann and Schweitzer, 1990; Billups et al., 2016), with the ratio between dextral and sinistral specimens used as a proxy for the water column structure (e.g., the depth of the thermocline) (Feldmeijer et al., 2014; Billups et al., 2016). *Globorotalia truncatulinoides* sinistral prefers warmer and less productive waters with a more stable and deeper thermocline (e.g., the center of the gyre system; Herman, 1972; Billups et al., 2016). Conversely, *Globorotalia truncatulinoides* dextral is documented to prefer a shallower habitat in the water column and is associated with cooler and more

productive waters (Feldmeijer et al., 2014; Billups et al., 2016). In cluster 2, *Globorotalia truncatulinoides* dextral and sinistral exhibit similar abundances (~ 6 %), indicating the presence of paleoecological conditions which favor both coiling types. This is in agreement with the proposed paleoenvironmental model for cluster 2, as the persistence of normal BOC and the absence of water mixing with SACW resulted in the presence of cold-water temperature and a relatively stable thermocline in the region. PCA analysis further supports the paleoceanographic conditions interpreted for cluster 2 (Fig. S1), with PC2 recording cold, relatively stable water column conditions and ABF in a more northern position, as suggested by the negative and positive loadings of *Globoconella inflata* and *Globorotalia crassaformis*, respectively.

- *Limited SACW intrusions (cluster 1b)*. The increase in abundance of *Globorotalia crassaformis* (14.26 %) and the concomitant decrease in *Globoconella inflata* (23.68 %) points to a southward shifting of the ABF with consequent mixing between the warm SACW and the colder BOC. Our data suggest that the intensity of water mixing was sufficient to promote a weak instability of the thermocline (Fig. 6). This interpretation is corroborated by a sharp increase in the abundance of *Globorotalia truncatulinoides* sinistral compared to dextral, as indicated by relative abundance data and negative values of the *Globorotalia truncatulinoides* coiling ratio. The dominance of the sinistral variant is due to the fact that the low amount of water mixing caused a small increase in the instability of the thermocline and induced a rise in water temperature.
- *Expanded SACW intrusions (cluster 1a)*. The abundance of *Globorotalia crassaformis* and *Globoconella inflata* continues to increase (18.37 %) and decrease (20.83 %), respectively. These data indicate an expansion of the SACW within the Benguela region, which, in turn, leads to a stronger water mixing, producing a higher thermocline instability compared to cluster 1b (Fig. 6). *Globorotalia truncatulinoides* dextral and sinistral again exhibit similar abundances (3.14 % and 1.48 %). This is because the water mixing produces a strong instability of the thermocline (favoring the dextral form) but at the same time induces a higher increase in water temperature (preferred by the sinistral variant) than that observed for cluster 1b. PCA results indicate the southern shifting of the ABF and the increase in water mixing (Table S5). PC3 is positively linked with *Globorotalia crassaformis* and negatively related to *Globoconella inflata*, reflecting the southward movement of the ABF. Moreover, the positive and negative loadings of *Globorotalia truncatulinoides* dextral and sinistral highlight the variations in the intensity of

the water column instability, which have a higher impact on the dextral type (Fig. 6).

- *Agulhas Leakage within the Benguela system (cluster 3)*. The planktonic foraminiferal assemblage shows an increase in tropical taxa, among which *Globorotalia menardii* exhibits the highest abundances (~ 20 %). Previous studies (Peeters et al., 2004; Caley et al., 2012; Villar et al., 2015) hypothesized that the tropical fauna in the southeastern Atlantic represents a reseeding population from the Indian Ocean. Specifically, giant eddies of warm water from the Agulhas Current can access the Benguela region according to a mechanism known as the Agulhas Leakage (Fine et al., 1988; Petrick et al., 2015; Friesenhagen, 2022). The variation in the intensity of the Agulhas Leakage through time allows the tropical fauna to overcome oceanographic barriers (e.g., the STC; Fig. 2; Friesenhagen, 2022) and enter the Atlantic Ocean. Chaisson and Ravelo (1997) proposed an alternative scenario, asserting that changes in wind stress directions between the eastern and western sides of the Atlantic Ocean during the Pleistocene induced a deepening and a shoaling of the thermocline in the western and eastern Atlantic, respectively. This would promote more favorable conditions for *Globorotalia menardii* in the eastern region of the Atlantic gyre, as this thermocline species responds to variation in the vertical water column stratification (Fairbanks et al., 1982; Curry et al., 1983; Friesenhagen, 2022). Our data indicate that the abundance trend of *Globorotalia menardii* does not consistently change with the *Globorotalia truncatulinoides* coiling ratio (Fig. 4), which, in turn, reflects variations of the thermocline in the water column (Feldmeijer et al., 2014; Billups et al., 2016). Moreover, PCA results show that *Globorotalia menardii* dominates the positive loading of PC1, with *Globorotalia crassaformis* showing negative scores (Table S5). Finally, the ALE index (Fig. 5; Table S3) only shows higher values (~ 33 %) in cluster 3, indicating an increase in Indian Ocean tropical fauna. Overall, our results assert that *Globorotalia menardii* cannot be part of the SASG domain because, in this case, the variation in abundance of the taxon should respond to changes in the thermocline. *Globorotalia menardii* is also not a constituent of the Angola subtropical fauna, as it is statistically not positively correlated to *Globorotalia crassaformis*. The increment of the Indian Ocean tropical taxa detected with the ALE index lends further support to the hypothesis that the Agulhas Leakage process is responsible for the reseeding of these tropical species in the southeastern Atlantic realm.

The record of a subtropical Indian Ocean fauna in Hole U1575A indicates that the strength of the Benguela Current must have been strong enough to allow the Agulhas eddies to reach the northernmost area of the BUS. In

fact, a greater ingress of Agulhas waters within the BUS may be favored by an intense BOC and a more southern position of the subarctic front (Garzoli et al., 1996; McClymont et al., 2005; Peeters et al., 2004).

The input of large Agulhas eddies in the system can cause variations in the water column structure, affecting the thermocline (Klein and Lapeyre, 2009). Specifically, in the Southern Hemisphere, anticyclonic (cyclonic) eddies induce a shoaling (deepening) of the thermocline. In the southeastern Atlantic Ocean, intermixing of anticyclonic warm eddies from the Agulhas Current with the cold Benguela Current can produce instability in the water column and shoal the thermocline. This process is possibly recorded by PC1, which indicates positive loadings for *Globorotalia truncatulinoides* dextral and *Globorotalia menardii* and negative scores for *Globorotalia truncatulinoides* sinistral.

4.2.2 Hole U1576A

Cluster analysis for Hole U1576A resulted in two major clusters, with cluster 1 separated into subclusters 1a and 1b. The paleoenvironmental conditions associated with each cluster are discussed below (Figs. 3–5; Tables S3 and S4).

- *Expanded SACW intrusions (cluster 1a)*. The foraminiferal assemblage of cluster 1a is characterized by high abundances of *Globorotalia crassaformis* (17.43 %) and slightly lower values of *Globoconella inflata* (17.18 %) compared to clusters 1b and 2. The increase in abundance of *Globorotalia crassaformis*, with lower amounts of *Globoconella inflata*, indicates the expansion of the SACW within the Benguela system, as also observed in Hole U1575A. However, the difference in abundance between *Globorotalia crassaformis* and *Globoconella inflata* is not as marked as in Hole U1575A, since Site U1576 is located further offshore, where the effect of the BOC is less pronounced.

Globorotalia truncatulinoides dextral and sinistral show similar abundances (5.09 % and 4.03 %). We believe that the close abundances of the dextral and sinistral variants are likely not linked to a strong instability of the thermocline, enhanced by the intrusions of warm SACW (as observed for Hole U1575A). This is confirmed by PCA results which highlight a negative correlation between *Globorotalia crassaformis* and both *Globorotalia truncatulinoides* dextral and sinistral (Fig. S2). A possible explanation could be the peculiar position of Hole U1576A, which is located in a more southern position and closer to the center of the gyre compared to Hole U1575A. Specifically, it lies in an area where the more temperate distal portion of the BOC encounters the warm waters of the sub-

tropical gyre. This area is then characterized by relatively warmer waters (favoring the sinistral variants) but also by the mixing between the BOC and the subtropical gyre waters (a condition preferred by the dextral form of *Globorotalia truncatulinoides*). Waters entering from the Angola Basin (SACW) were probably already mixed with the Benguela Current before reaching the latitudinal position of Hole U1576A and cannot have a strong impact on the thermocline stability (as instead observed for Hole U1575A).

- *Agulhas Leakage within the Benguela system (cluster 1b)*. Hole U1576A also recorded phases of increase in the Agulhas Leakage (Fig. 5; Table S4). The ALE index shows higher values (~30 %) for this cluster, corresponding to an increase in the Indian Ocean tropical taxa within the assemblage. As observed for Hole U1575A, the abundance trend of *Globorotalia menardii* does not follow the change in the ratio between *Globorotalia truncatulinoides* dextral and sinistral. Thus, the variation in abundance of *Globorotalia menardii* is not linked to changes in the regional thermocline.

Similarly to Hole U1575A, PCA results here also show positive loadings for *Globorotalia menardii* and *Globorotalia truncatulinoides* dextral but a negative loading for *Globorotalia truncatulinoides* sinistral. This can again be explained by the instability of the thermocline linked to the mixing between the Agulhas eddies with the Benguela waters. However, thermocline variability was less pronounced than in Hole U1575A. This is indicated by the lower PCA loading values of *Globorotalia truncatulinoides* dextral than those observed in Hole U1575A. We believe that the location of Hole U1576A (closer to the center of the gyre) could again play an important role in explaining the subtle variations in the thermocline for this site. In fact, warm Agulhas eddies mix with already more temperate waters of the BOC, producing a smaller impact on the thermocline.

- *Nutrient filaments within the BOC (cluster 2)*. This foraminiferal assemblage is dominated by *Globoconella inflata*, with common occurrences of *Globorotalia truncatulinoides* sinistral (12.56 %), *Neogloboquadrina incompta* (13.16 %), and *Orbulina universa* (11.12 %). SIMPER analysis indicates that the main species responsible for the clustering are *Orbulina universa*, *Globorotalia truncatulinoides* sinistral and dextral, and *Neogloboquadrina incompta*. Moreover, according to PCA results, the same species show the highest positive and negative loading scores for PC3.

The taxon *Orbulina universa* can inhabit tropical, subtropical, and transitional water masses (Bé and Tolderlund, 1971; Schiebel and Hemleben, 2017) and can pre-

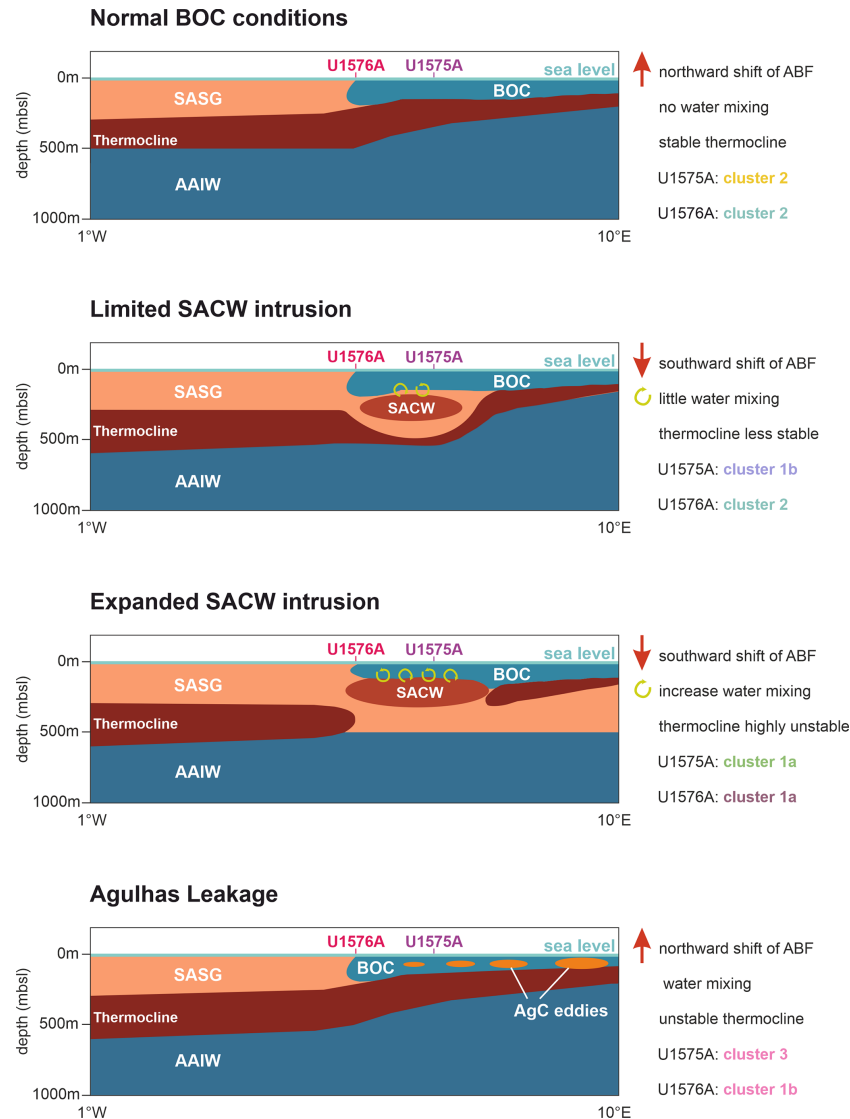


Figure 6. Conceptual model showing the interaction between the SACW, BOC, and AgC water masses in the studied area. BOC: Benguela Oceanic Current; SACW: South Atlantic Central Water; SASG: South Atlantic Subtropical Gyre waters; AAIW: Antarctic Intermediate Water; AgC: Agulhas Current. The clusters for Holes U1575A and U1576A associated with each paleoceanographic condition are also indicated. The local thermocline is represented as a dark-orange area.

fer waters with moderate nutrient levels (van Leeuwen, 1989; Giraudeau, 1993; Lombard et al., 2011; Ufkes and Kroon, 2012). This species was commonly found in the northern Benguela region, south of the ABF (Brenner, 1983; Herbert, 1987), and restricted to a latitudinal range of about 17–25° S (Giraudeau, 1993). However, this study confirmed its presence until at least 24° S.

A previous study from Giraudeau (1993) indicated that the increase in abundance of *Orbulina universa* can be linked to the concomitant presence of warmer (> 18 °C) and more nutrient-rich conditions in the area. This paleoenvironmental interpretation is corroborated by our results, showing a foraminiferal assemblage character-

ized by common *Orbulina universa* and species indicative of the less fertile offshore waters typical of the BOC (*Globorotalia inflata*, *Globigerina bulloides*, and *Neogloboquadrina incompta*). Moreover, the presence of common *Globorotalia truncatulinoides* sinistral supports the warmer-water conditions (Fig. 5; Herman, 1972; Billups et al., 2016) at the site. PC3 (Fig. S2) indicates that the highest and opposite loadings are associated with *Neogloboquadrina incompta* (positive scores) and *Orbulina universa* (negative scores). *Neogloboquadrina incompta* thrives in the BOC and prefers temperatures between 10 and 18 °C. The co-existence of both species supports the presence of temperate and rel-

atively nutrient-enriched waters. Interestingly, *Globorotalia truncatulinoides* dextral exhibits a negative score, as this coiling variant prefers more productive waters (Billups et al., 2016). However, *Globorotalia truncatulinoides* sinistral shows a higher abundance because, although preferring less fertile waters, it thrives in warmer water masses away from the continental margin.

We believe that the assemblage of cluster 2 may reflect episodes of nutrient filaments transported offshore from the coastal upwelling zone. Ufkes et al. (2000) and Ufkes and Kroon (2012) detected phases of extreme coastal upwelling events in the northern BUS during the Pleistocene, possibly linked to powerful zonal winds. Those strong winds could transport a small part of the nutrients, upwelled along the coast, further offshore within the more oligotrophic portion of the northern BUS.

4.3 Paleooceanographic evolution of the northern BUS during the Quaternary

The planktonic foraminiferal records in Holes U1575A and U1576A indicate large-scale variability in the paleoenvironmental conditions since the Early Pleistocene (Figs. 6–7). Specifically, we observed an alternation of periods reflective of variations in the ABF positions, Agulhas intrusions from the Indian Ocean, and an increase in the nutrient transport offshore, further away from the coastal upwelling center. Those paleooceanographic conditions were sporadically recorded within the whole analyzed time interval (Fig. 7).

Intervals of the ABF shifting were recorded several times at both sites, within the studied stratigraphic sequences (between 0.43 and 1.30 Myr; Fig. 7). Particularly, its southward (northward) movements indicate the intrusion (absence) of the warm SACW within the northern sector of the BUS. Several authors (Walter, 1937; Boyd and Thomas, 1984; Boyd et al., 1987; Shannon and Nelson, 1996) linked the southern–northern shift of the ABF to the interannual Benguela Niño/Niña phenomena. During the Benguela Niño (Niña) events, an increase (decrease) in sea surface temperatures (SSTs) occurs in the eastern equatorial and southeastern Atlantic Ocean due to the relaxation (intensification) of the trade winds (Rouault et al., 2007; Rosell-Melé et al., 2014; Illig and Bachèlery, 2024). The reduction in intensity of the trade winds during the Benguela Niño induces warmer SST in the equatorial Atlantic and the ingress of warm Angola waters in the BUS (Hisard, 1980; Philander, 1990; Illig et al., 2004). The opposite situation occurs during the Benguela Niña, when SSTs decrease and no SACW expands in the Benguela system. Thus, the Benguela Niño/Niña events have a strong impact on the upwelling intensity and water mixing (Boyer et al., 2001; Imbol Koungue and Brandt, 2021). Benguela Niño events are regarded as the Atlantic counterpart of the widely-known Pacific El Niño–Southern Oscillation (ENSO; Bjerknes, 1969), which is linked to changes in

the wind strength due to variations in the atmospheric circulation patterns in the Pacific Ocean (Qiu and Chen, 2010; Kaboth-Bahr and Mudelsee, 2022). However, it is important to note that no conclusive evidence exists that the Atlantic Benguela Niño can be in phase with the Pacific ENSO (Shannon and Nelson, 1996). In fact, they may reflect different forcing processes (Rosell-Melé et al., 2014). Modern SST data (Gammelsrød et al., 1998; Rouault et al., 2007) from the Angola and Cape basins indicate intervals of higher sea-surface temperatures interpreted as the result of Benguela Niño events in the region. Records of SST reconstruction in the BUS during the Pliocene–Pleistocene time intervals (Marlow et al., 2000; Schefuß et al., 2004; Etourneau et al., 2009; Rosell-Melé et al., 2014) also support the possible existence of Benguela Niño-like conditions in the region. In particular, Rosell-Melé et al. (2014) promoted the presence of a persistent Benguela Niño-like state before 3.5 Ma in the Pliocene due to the existence of warm SSTs (Salzmann et al., 2011) and a more reduced meridional temperature gradient (Fedorov et al., 2010). The Pleistocene period was characterized by the Early–Middle Pleistocene transition (EMPT; 1.4–0.4 Myr), during which a switch from a 41 to 100 kyr orbital cycle occurred (Berger and Jansen, 1994; Head and Gibbard, 2015; Herbert, 2023).

During this time interval, the presence of high-amplitude SST glacial–interglacial variability and the increase in the meridional thermal gradient could likely promote an alternation of possible Benguela Niño/Niña conditions (Christensen and Giraudeau, 2002; Etourneau et al., 2009; Martinez-Garcia et al., 2010; Rosell-Melé et al., 2014). The planktonic foraminiferal dataset for Holes U1575A and U1576A detected phases of southward–northward shifts in the ABF (up to 24°35′ S), between 0.43 and 1.30 Myr, within the part of the studied stratigraphic sequence corresponding to the EMPT (Fig. 7; Tables S1–S2). Here, the southern extension of the ABF was accompanied by phases of limited/expanded SACW ingressions and their mixing with the more temperate waters of the BOC (Figs. 6 and 7).

Specifically, our data for Hole U1575A indicate that, between 0.91 and 0.61 Myr, most of the sediment record exhibits an alternation between normal Benguela conditions (with stable regional thermocline) and only limited SACW intrusions (slightly reduced thermocline stability) within the BUS (Figs. 3, 6, and 7), as inferred by low abundances of the species *Globorotalia crassaformis* (Fig. 3). Alkenone-based SST reconstruction north of the ABF (Schefuß et al., 2004) revealed a pronounced SST minimum around 0.90 Ma, with a slow SST increase until 0.60 Ma (Fig. 7). The trend in decreasing SST can also be observed in the southern Benguela (Petrick et al., 2015) and northern Benguela upwelling regions (Etourneau et al., 2009; Fig. 7). Thus, we can conclude that the paleoenvironmental settings inferred from the analysis of the planktonic assemblage (between 0.90 and 0.61 Myr) are indicative of a period of low SST and associated Benguela Niña conditions. The persistence

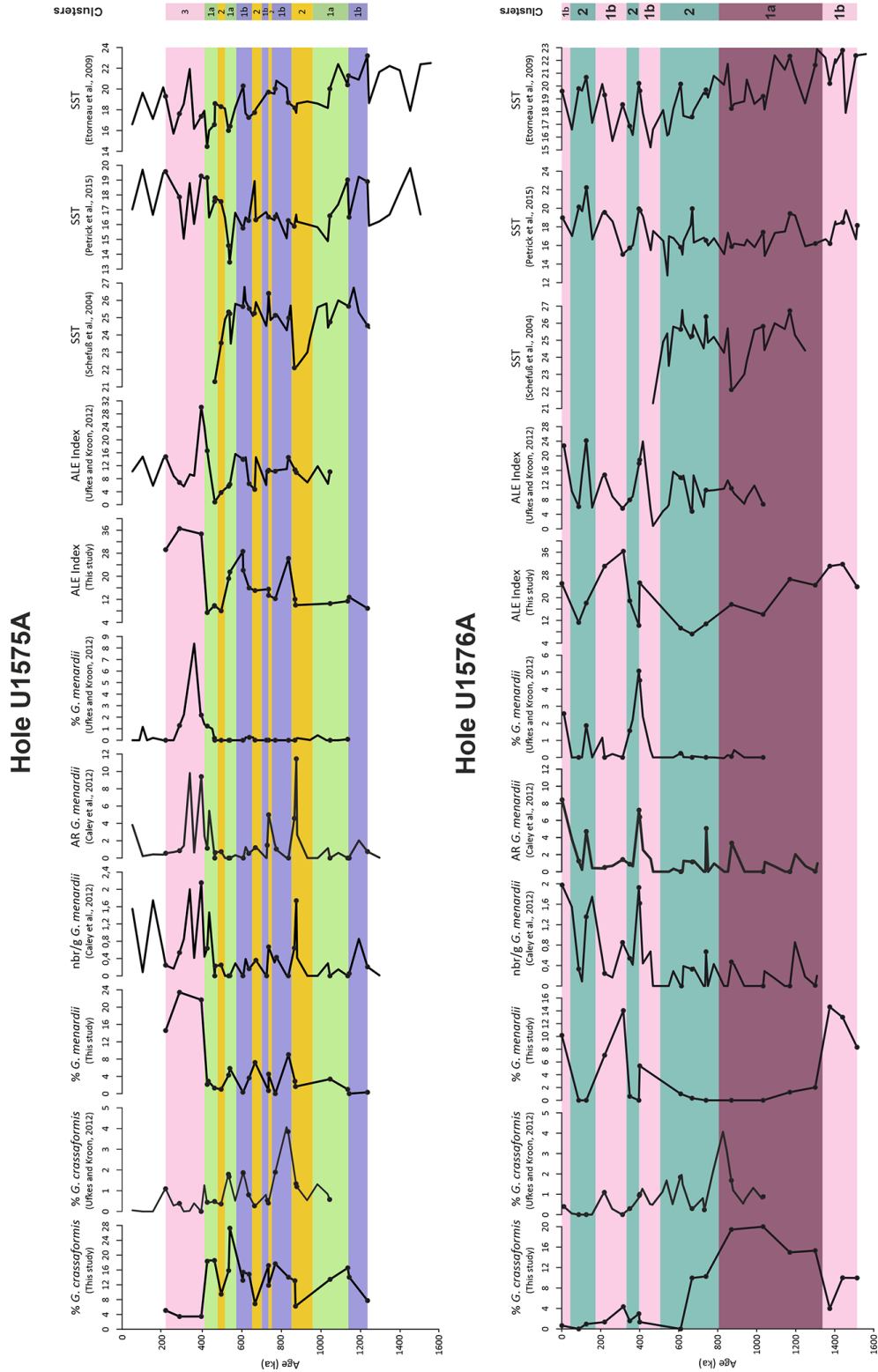


Figure 7. Correlation of planktonic foraminiferal data from Holes U1575A and U1576A (converted to age) with the abundance dataset from Ufkes and Kroon (2012) and Caley et al. (2012) as well as SST records from Schefuß et al. (2004), Etorneau et al. (2009), and Petrick et al. (2015). All data are plotted together with the intervals obtained from cluster analysis. The ALE index for Ufkes and Kroon (2012) was calculated based on their assemblage data, following Caley et al. (2014). The abundance of *G. menardii* for the Caley et al. (2012) record is expressed as both concentration (number of specimens per gram of bulk sediment) and accumulation rate (AR = number of specimens $\text{cm}^{-2} \text{ka}^{-1}$). SST values are indicated in degrees Celsius ($^{\circ}\text{C}$). The black dots indicate the age of the samples analyzed in this study.

of Benguela Niña-like phases, in turn, limited the southward ABF shifting and the expansions of the warm SACW into the northern Benguela region. The same conclusions cannot be drawn from Hole U1576A due to a lower biostratigraphic resolution achieved for the abovementioned time interval. Instead, the extended ABF expansion and related high thermocline instability were recorded at both sites prior to 0.90 and post 0.61 Ma, respectively (Fig. 7; Table S5). These paleoceanographic conditions can be inferred from high percentages of *Globorotalia crassaformis* and from an increase in the recorded SSTs in the Benguela region (Fig. 7). Similar results were published by Ufkes and Kroon (2012), who suggested recurrent ABF shifts within the EMPT (detected at Core T89-40), based on the increase in abundance of *Globorotalia crassaformis* (Fig. 7). Specifically, they detected a possible Benguela Niño-induced southward shift in the ABF front to 21° S. Our results align with the interpretation of Ufkes and Kroon (2012) and show that the ABF reached a more southern position (almost 25° S) during the EMPT. Interestingly, the percentages of *G. crassaformis* recorded by Ufkes and Kroon (2012) during the southward movements of the ABF consistently show lower values compared to what was observed in our record during the same paleoceanographic conditions (Fig. 7). The difference in percentage can be related to the position of Core T89-40, which, according to the modern oceanographic configuration, is located in a region of the northern BUS actively influenced by a cold tongue of upwelled waters transported offshore (Ufkes et al., 2000). This condition could also have been present at Core T89-40 during the EMPT, as Ufkes and Kroon (2012) detected high abundances of typical upwelling-related planktonic species (e.g., *Neogloboquadrina pachyderma*) in their record. The influx of colder upwelled waters can indeed obscure the ABF signal at Core T89-40, by limiting the ingression of the warm SACW.

At Site U1576, we also recorded phases of nutrient filaments transported offshore since the Early–Middle Pleistocene (starting from 0.74 Ma; Fig. 7), which may reflect intense coastal upwelling events. This would have been possible during glacial stages, when the ABF is located north of the BUS (thus reducing or impeding the intrusions of SACW) and the SE trade winds intensify, enhancing the upwelling intensity (Manabe and Broccoli, 1985; Jansen et al., 1996; Schefuß et al., 2004). In particular, the upwelling intensification events recorded at Hole U1576A (within the interval 0.91–0.61 Myr) may be linked with the establishment of La Niña-like conditions in the northern BUS, when lower SSTs and the northern position of the ABF promoted strong upwelling episodes (Fig. 7).

During the last 0.6 Myr, the southeastern Atlantic Ocean experienced warmer SSTs in both the north (Etourneau et al., 2009, 2010) and south (Petrick et al., 2015) sectors of the BUS (Fig. 7), with an increase in the influx of AgC waters within the Benguela region during deglaciation phases (Peeters et al., 2004; Martínez-Méndez et al., 2008; Dick-

son et al., 2010; Marino et al., 2013; Caley et al., 2014; Petrick et al., 2015). Conversely, the leakage of the AgC in the Atlantic Ocean was limited during glacials (Biaščoch et al., 2008; Bard and Rickaby, 2009). Peeters et al. (2004) and Caley et al. (2012, 2014) observed an increase in the abundance of the warm species *Globorotalia menardii* at ODP Site 1087 (Fig. 7), located in the southern sector of the BUS, near the Agulhas retroflection area. Here, the higher amount of *Globorotalia menardii* was interpreted as reflective of the intrusions of the Agulhas waters in the BUS prior to interglacial maxima (Petrick et al., 2015, 2018). Similarly, at both sites, the youngest part of our record (since 0.61 Ma) showed intervals of increase in the percentages of *G. menardii*, which is in agreement with the abundances and the ALE index values observed in Ufkes and Kroon (2012) and Caley et al. (2014; Fig. 7). Clearly, our record statistically demonstrated that the presence of *G. menardii* within the BUS is related to the Agulhas Leakage and is not part of the SASG system (see Sect. 4.2). Thus, we detected inputs of Agulhas eddies in the northern Benguela region and associated thermocline shoaling in the BUS (Figs. 3 and 5), which may correspond to the previously described deglaciation events detected in the southern sector. We can, therefore, hypothesize that, during deglaciations, the position of the subpolar front was sufficiently south to allow the ingression of the warm Agulhas eddies in the BUS. Furthermore, prior to interglacial maxima, the SSTs are still low enough to limit the shift in the ABF southward, allowing the BOC to have sufficient strength to carry the Agulhas eddies to the northernmost area of the BUS.

Interestingly, Caley et al. (2012) detected an increase in *G. menardii* around 0.87 Ma at IODP Site 1087, while our record instead showed low percentages of *G. menardii* and the presence of normal BOC conditions in the northern BUS. Furthermore, the trend in abundance of *G. menardii* recorded by Ufkes and Kroon (2012) is in agreement with our data (Fig. 7), although it shows lower percentages due to the persistence of the cold tongue at Core T89-40. A possible reason for the detection of higher *G. menardii* at IODP Site 1087 could be related to the fact that their site is located in the southern Benguela region, close to the AgC retroflection area. Specifically, this site could register the limited ingressions of the AgC eddies during colder time intervals, when the subpolar front extended north.

Sediments from Hole U1576A also recorded inputs of warm Indian Ocean waters through the Agulhas Leakage in the Early Pleistocene (between 1.58 and 1.30 Ma; Figs. 3 and 4). Previous studies (Franzese et al., 2006; Caley et al., 2012, 2014; Petrick et al., 2015; Fig. 7) provided robust records of the Agulhas Leakage from 0.5 Ma to present, based on SST, salinity, and foraminiferal assemblage datasets (Petrick et al., 2018). However, limited data were produced before 0.5 Ma in the BUS, with only Caley et al. (2012) extending the studied record to 1.35 Ma (Fig. 7). Furthermore, the variations in the ACC from the Pliocene–Pleistocene transition and their ef-

fect on the Agulhas Leakage are still poorly known (Keany and Kennett, 1972; Hodell et al., 2000; Becquey and Gersonde, 2002; Diekmann and Kuhn, 2002). Singh and Sinha (2021) attempted to detect the shifts in the ACC spanning the last 2.6 Ma, with no northward movements observed prior to 1.2 Ma. Based on this evidence, we suggest that the Agulhas Leakage signal observed in our study between 1.58 and 1.30 Ma may correspond to a period of deglaciation (as also suggested by higher SST values; Fig. 7), during which the polar front was not moving northwards, allowing Agulhas eddies to reach the southeastern Atlantic Ocean.

5 Conclusions

In this study, we analyzed planktonic foraminifera assemblages from IODP Expedition 391, Holes U1575A and U1576A, located on the northwestern sector of the Tristan–Gough–Walvis Ridge (TGW) track in the southeastern Atlantic Ocean. The sites are situated in the northern area of the Benguela Upwelling System (BUS) and are influenced by the Benguela Oceanic Current (BOC). The principal aim of this research was to investigate changes in the local paleoceanographic conditions since the onset of the Early–Middle Pleistocene transition (EMPT), based on the analysis of the planktonic foraminiferal assemblages and on the application of the Agulhas Leakage efficiency (ALE) index and the *Globorotalia truncatulinoides* dextral / sinistral coiling ratio:

1. Age investigation based upon the calcareous nannofossils and planktonic foraminiferal content allowed us to establish a reliable biostratigraphic framework (covering the Early–Middle to Late Pleistocene) for the paleoecological interpretations of Holes U1575A and U1576A.
2. Cluster analysis on the planktonic foraminifera assemblages produced three main clusters for Hole U1575A and two major clusters for Hole U1576A, with cluster 1 subdivided into two subclusters (1a and 1b) at both sites. Overall, those clusters represent different paleoceanographic conditions during the Pleistocene, reflecting phases of northward–southward shifts in the ABF, normal BOC conditions, increased offshore nutrient transport, and intrusions of the Agulhas waters from the Indian Ocean. The paleoecological interpretation of the clusters is further supported by PCA results.
3. The northward–southward migrations of the ABF were detected based on the abundance of *Globorotalia crassaformis* compared to *Globorotalia inflata*. Specifically, a concomitant increase in *Globorotalia crassaformis* and a reduction in the abundance of *Globoconella inflata* indicated a southward shift in the ABF and consequent ingressions of SACW within the northern sector of the BUS. Contrarily, normal BOC conditions with no SACW mixing were corroborated by higher values of

Globoconella inflata and low abundances of *Globorotalia crassaformis*.

4. *Globorotalia truncatulinoides* dextral / sinistral coiling ratio and their abundance data reflected changes in the stability of the thermocline, temperature, and productivity at the studied sites. During phases of southward movements of the ABF, a higher increase in the abundance of *Globorotalia truncatulinoides* sinistral compared to dextral, along with a negative coiling ratio, were indicative of reduced water mixing between the BOC and the SACW, causing a slight decrease in the thermocline stability and a rise in water temperature. Conversely, similar abundances of *Globorotalia truncatulinoides* dextral and sinistral and a more positive value of the coiling ratio suggested stronger water mixing (leading to a stronger instability of the local thermocline than observed in cluster 1b) and a higher increase in water temperature. Periods of normal BOC conditions, with no intrusions of the SACW in the BUS, showed the presence of a relatively stable thermocline with colder water temperature, which favored both coiling types. Furthermore, in Hole U1576A, the higher abundance of *Globorotalia truncatulinoides* sinistral was also interpreted as indicative of less fertile waters within the BOC.
5. The local thermocline response is strictly related to longitudinal and latitudinal variations in the oceanographic conditions in the studied area. This can be seen in Hole U1576A, which is situated in a more southern position and closer to the center of the gyre, compared to Hole U1575A. Thus, we observed only a subtle thermocline variability as the warm SACWs and Agulhas eddies mix with already more temperate waters within the BUS.
6. The ALE index, together with the analyses of the planktonic foraminifera assemblage and the *Globorotalia truncatulinoides* coiling ratio, support the interpretation that *Globorotalia menardii* and the other tropical taxa represent a reseeding population from the Indian Ocean, associated with the Agulhas Leakage. Higher (lower) values of the ALE index indicate enhanced (reduced) transport of Indian Ocean warm waters within the BUS. This study further proved the reliability of the ALE index in successfully tracing the input of the Agulhas waters in the northernmost sector of the BUS.
7. A sharp increase in the abundance of *Orbulina universa* in Hole U1576A indicates the existence of temperate and moderately nutrient-enriched waters, which can be explained by the transport of nutrient filaments offshore, far from the coastal upwelling area.
8. The planktonic foraminifera dataset at both sites recorded phases of ABF shift and periods of increase in the Agulhas Leakage from the EMPT to the recent.

Southwards–northwards movements of the ABF were interpreted as reflecting long-term changes in the occurrence of Benguela Niño/Niña events in the SE Atlantic Ocean. In particular, between 0.91 and 0.61 Myr, we detected intervals of possible Niña-like conditions in the northern BUS, corresponding to periods of low SSTs recorded in the region from previous studies. Instead, phases of Agulhas water intrusions in the BUS may be associated with deglaciation stages since the onset of the EMPT.

Appendix A

Plate A1 showing the relevant calcareous nannofossil species used as biostratigraphic indicators in Holes U1575A and U1576A.

Plates B1–B5 illustrating the main planktonic foraminifera species used for biostratigraphic and paleoceanographic interpretations of Holes U1575A and U1576A.

Plate A1

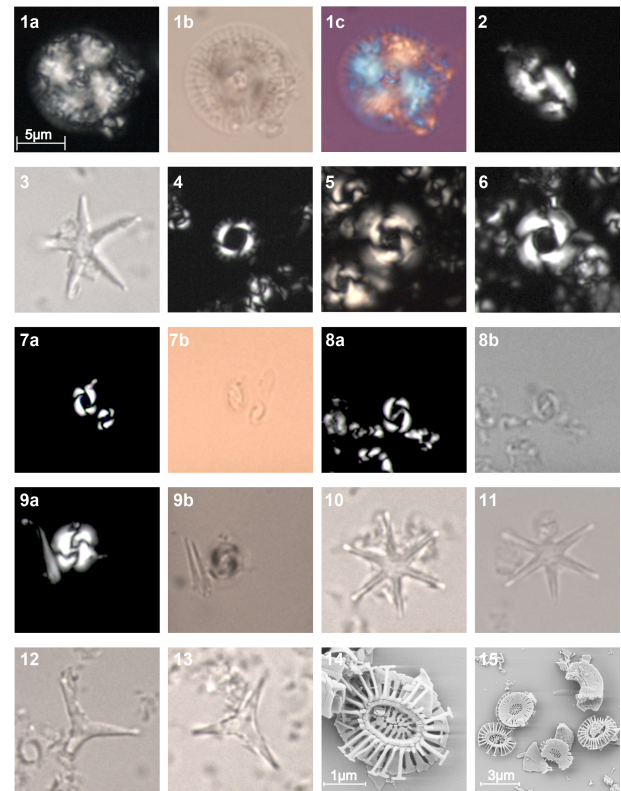


Plate A1. (1) *Calcidiscus macintyreii*, Sample U1575A-5R-7W, 0–2 cm. (1a) LM, X nicols; (1b) LM, FC; (1c) LM, quartz wedge interference image. (2) *Helicosphaera sellii*, Sample U1575A-5R-3W, 0–2 cm. LM, X nicols. (3) *Discoaster asymmetricus*, Sample U1575A-5R-7W, 0–2 cm. LM, X nicols. (4) *Pseudoemiliania lacunosa*, Sample U1576A-3R-3W, 145–147 cm. LM, X nicols. (5–6) *Reticulofenestra asanoi*, Sample U1575A-3R-6W, 0–2 cm. LM, X nicols. (7) Small *Gephyrocapsa* spp. (< 4 µm), Sample U1575A-1R-2W, 0–2 cm. (7a) LM, X nicols; (7b) LM, FC. (8) Medium *Gephyrocapsa* spp. (4–4.5 µm), Sample U1575A-1R-1W, 0–2 cm. (8a) LM, X nicols; (8b) LM, FC. (9) Large *Gephyrocapsa* spp. (> 5.5 µm), Sample U1575A-4R-3W, 88–90 cm. (9a) LM, X nicols; (9b) LM, FC. (10–11) *Discoaster brouweri*, Sample U1576A-4R-3W, 0–2 cm. LM, FC. (12–13) *Discoaster triradiatus*, Sample U1576A-4R-3W, 0–2 cm. LM, FC. (14–15) *Emiliana huxleyi*, Sample U1576A-1R-1W, 0–2 cm. SEM.

Appendix B

Plate B1

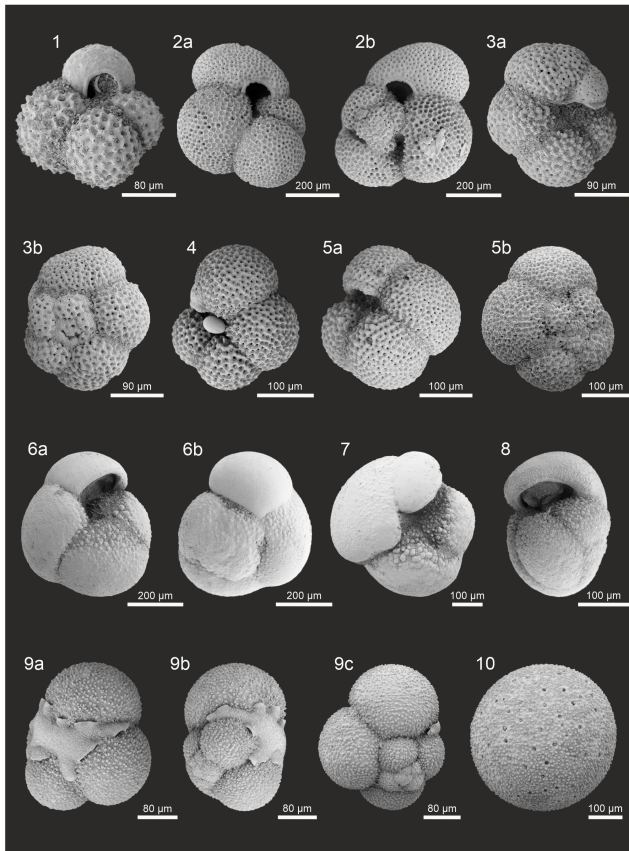


Plate B1. (1) *Globoturborotalita rubescens*, Sample U1576A-1R-3W, 60–62 cm. (2) *Trilobatus sacculifer*, Sample U1576A-1R-3W, 60–62 cm. (2a) Umbilical view; (2b) spiral view. (3) *Neogloboquadrina pachyderma*, Sample U1576A-1R-3W, 60–62 cm. (3a) Umbilical view; (3b) spiral view. (4) *Neogloboquadrina incompta*, Sample U1576A-1R-3W, 60–62 cm. Umbilical view. (5) *Neogloboquadrina incompta*, Sample U1576A-1R-3W, 60–62 cm. (5a) Umbilical view; (5b) spiral view. (6) *Globoconella inflata*, Sample U1576A-1R-7W, 58–60 cm. (6a) Umbilical view; (6b) spiral view. (7) *Globoconella inflata*, Sample U1576A-1R-7W, 58–60 cm. Umbilical view. (8) *Globoconella inflata*, Sample U1576A-3R-6W, 10–12 cm. Side view. (9) *Globigerinita glutinata*, Sample U1576A-1R-3W, 60–62 cm. (9a) Umbilical view; (9b) side view; (9c) spiral view. (10) *Orbulina universa*, Sample U1576A-1R-3W, 60–62 cm. All specimens were imaged at 3 kv and with an external secondary electron (SE) detector.

Plate B2

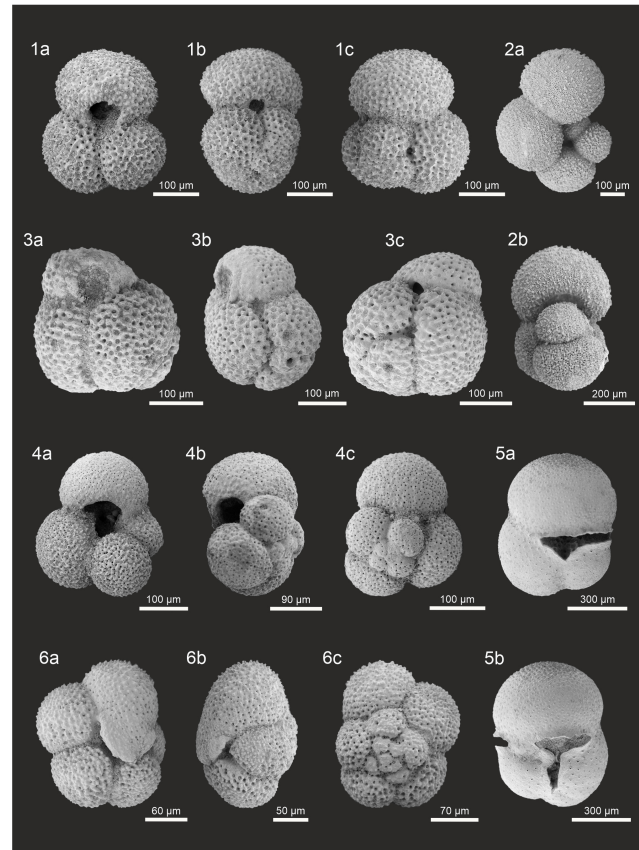


Plate B2. (1) *Globigerinoides ruber* s.s., Sample U1576A-1R-3W, 60–62 cm. (1a) Umbilical view; (1b) side view; (1c) spiral view. (2) *Globigerinella siphonifera*, Sample U1576A-3R-6W, 10–12 cm. (2a) Umbilical view; (2b) side view. (3) *Globigerinoides ruber* s.l., Sample U1576A-1R-3W, 60–62 cm. (3a) Umbilical view; (3b) side view; (3c) spiral view. (4) *Globigerina bulloides*, Sample U1576A-1R-3W, 60–62 cm. (4a) Umbilical view; (4b) side view; (4c) spiral view. (5) *Sphaeroidinella dehiscens*, Sample U1576A-1R-3W, 60–62 cm. (5a) Umbilical view; (5b) spiral view. (6) *Turborotalita quinqueloba*, Sample U1576A-3R-7W, 0–2 cm. (6a) Umbilical view; (6b) side view; (6c) spiral view. All specimens were imaged at 3 kv and with an external secondary electron (SE) detector.

Plate B3

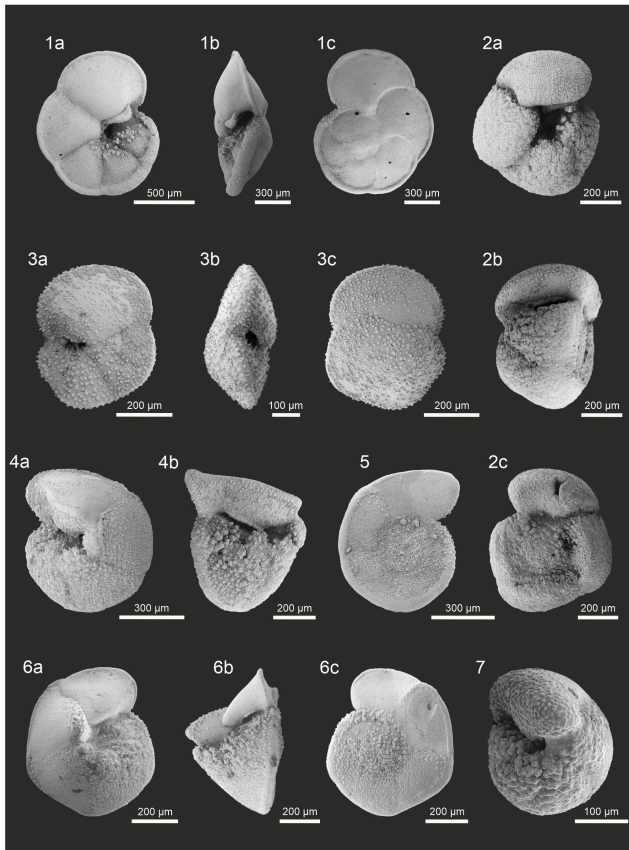


Plate B3. (1) *Globorotalia menardii*, Sample U1575A-3R-1W, 0–2 cm. (1a) Umbilical view; (1b) side view; (1c) spiral view. (2) *Globorotalia crassaformis*, Sample U1575A-3R-1W, 0–2 cm. (2a) Umbilical view; (2b) side view; (2c) spiral view. (3) *Globorotalia hirsuta*, Sample U1576A-1R-3W, 60–62 cm. (3a) Umbilical view; (3b) side view; (3c) spiral view. (4) *Globorotalia truncatulinoides* (dextral), Sample U1575A-1R-1W, 140–142 cm. (4a) Umbilical view; (4b) side view. (5) *Globorotalia truncatulinoides* (dextral), Sample U1575A-3R-4W cm, 138–140. Spiral view. (6) *Globorotalia truncatulinoides* (sinistral), Sample U1576A-1R-3W, 60–62 cm. (6a) Umbilical view; (6b) side view; (6c) spiral view. (7) *Globorotalia tosaensis*, Sample U1576A-3R-7W, 0–2 cm. Umbilical view. All specimens were imaged at 3 kv and with an external secondary electron (SE) detector.

Plate B4

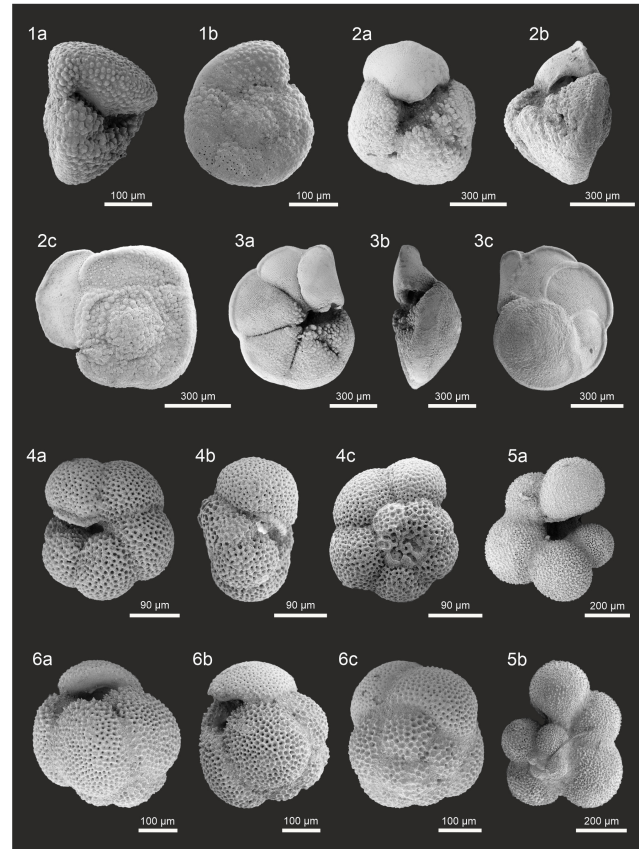


Plate B4. (1) *Globorotalia tosaensis*, Sample U1576A-3R-7W, 0–2 cm. (1a) Side view; (1b) spiral view. (2) *Globorotalia hessi*, Sample U1575A-1R-4W, 10–12 cm. (2a) Umbilical view; (2b) side view; (2c) spiral view. (3) *Globorotalia flexuosa*, Sample U1576A-2R-1W, 0–2 cm. (3a) Umbilical view; (3b) side view; (3c) spiral view. (4) *Neogloboquadrina acostaensis*, Sample U1575A-5R-4W, 135–137 cm. (4a) Umbilical view; (4b) side view; (4c) spiral view. (5) *Globigerinella calida*, Sample U1576A-1R-1W, 0–2 cm. (5a) Umbilical view; (5b) spiral view. (6) *Dentoglobigerina altispira*, Sample U1575A-5R-7W, 0–2 cm. (6a) Umbilical view; (6b) side view; (6c) spiral view. All specimens were imaged at 3 kv and with an external secondary electron (SE) detector.

Plate B5

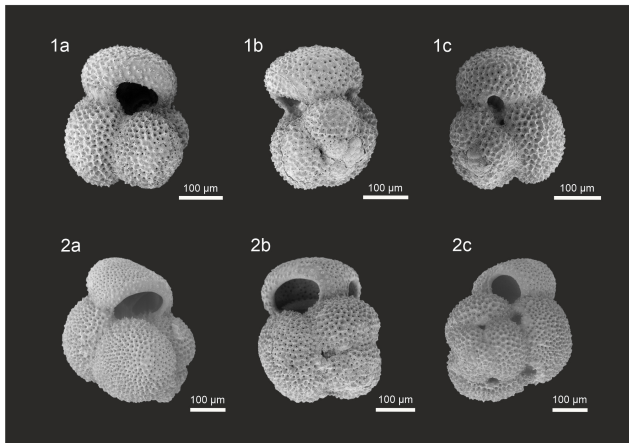


Plate B5. (1) *Globigerinoides obliquus*, Sample U1576A-4R-2W, 10–12 cm. (1a) Umbilical view; (1b) side view; (1c) spiral view. (2) *Globigerinoides extremus*, Sample U1576A-4R-3W, 0–2 cm. (2a) Umbilical view; (2b) side view; (2c) spiral view. All specimens were imaged at 3 kv and with an external secondary electron (SE) detector.

Code and data availability. The oceanographic map was made with Ocean Data View (Schlitzer, 2021) version 5.6.2, available at <https://odv.awi.de> (last access: 12 March 2024).

Statistical and ordination analyses were performed using PAST (version 4.09) (Hammer et al., 2001), available at <https://www.nhm.uio.no/english/research/resources/past/>.

The quantitative data that support the findings of this study are openly available in PANGAEA at <https://doi.org/10.1594/PANGAEA.965686> (Del Gaudio et al., 2024a) and <https://doi.org/10.1594/PANGAEA.965703> (Del Gaudio et al., 2024b).

Supplement. The supplement related to this article is available online at: <https://doi.org/10.5194/cp-20-2237-2024-supplement>.

Author contributions. All authors approved the paper and agreed to its submission. All authors discussed the results and provided critical feedback on the final version of the paper. AVDG designed the study. AVDG and AA processed and analyzed the samples. AVDG performed statistical analyses. WEP, GA, and WK supervised the research activity. WK was responsible for the funding acquisition.

Competing interests. The contact author has declared that none of the authors has any competing interests.

Disclaimer. Publisher's note: Copernicus Publications remains neutral with regard to jurisdictional claims made in the text, published maps, institutional affiliations, or any other geographical representation in this paper. While Copernicus Publications makes every effort to include appropriate place names, the final responsibility lies with the authors.

Acknowledgements. Samples and data provided by the International Ocean Discovery Program (IODP) were used for this research project. The authors would like to express their gratitude to all the personnel of the D/V *JOIDES Resolution* for their work during IODP Expedition 391 and the shipboard science party for collecting the shipboard data. All shipboard data are publicly available at <https://www.iodp.tamu.edu> (last access: 1 October 2024). The authors would like to thank the editor Erin McClymont and the two anonymous reviewers who kindly provided thoughtful comments on the paper. Also, the authors would like to acknowledge Benjamin Petrick for providing data resources. AVDG warmly thanks the Austrian Academy of Science (ÖAW) for providing funding to support her participation in IODP Expedition 391 as a shipboard scientist. AVDG would also like to express her gratitude to the Cushman Foundation for financially supporting this research project through the Cushman Foundation Student Travel Award.

Financial support. This research has been supported by the Austrian Science Fund (FWF) (grant no. P 31683-N29).

Review statement. This paper was edited by Erin McClymont and reviewed by two anonymous referees.

References

- André, A., Weiner, A., Quillévéré, F., Aurtas, R., Douady, C. J., de Garidel-Thoron, T., Escarguel, G., de Vargas, C., and Kuchera, M.: The cryptic and the apparent reversed: lack of genetic differentiation within the morphologically diverse plexus of the planktonic foraminifer *Globigerinoides sacculifer*, *Paleobiology*, 39, 21–39, <https://doi.org/10.1666/0094-8373-39.1.21>, 2013.
- Andrews, W. R. H. and Hutchings, L.: Upwelling in the southern Benguela Current, *Prog. Oceanogr.*, 9, 1–8, [https://doi.org/10.1016/0079-6611\(80\)90015-4](https://doi.org/10.1016/0079-6611(80)90015-4), 1980.
- Arrigoni, A., Piller, W. E., and Auer, G.: A new methodology for foraminifera extraction from cemented calcareous shelf sediments, *Mar. Micropaleontol.*, 187, 102324, <https://doi.org/10.1016/j.marmicro.2023.102324>, 2023.
- Aubry, M.-P.: Handbook of Cenozoic Calcareous Nannoplankton: Book 1, Ortholithae (Discoasters), *Micropaleontology Press*, New York, 1984.
- Aubry, M.-P.: Handbook of Cenozoic Calcareous Nannoplankton: Book 2, Ortholithae (Holococcoliths, Ceratoliths, Ortholiths and Others), *Micropaleontology Press*, New York, 1988.
- Aubry, M.-P.: Handbook of Cenozoic Calcareous Nannoplankton: Book 3, Ortholithae (Pentaliths, and Others), Heliolithae (Fasciculiths, Sphenoliths and Others), *Micropaleontology Press*, New York, 1989.

- Aubry, M.-P.: Handbook of Cenozoic Calcareous Nannoplankton: Book 4, Helicolithae (Helicoliths, Cribriliths, Lopadoliths and Others), Micropaleontology Press, New York, 1990.
- Auer, G., De Vleeschouwer, D., Smith, R. A., Bogus, K., Groeneveld, J., Grunert, P., Castañeda, I. S., Petrick, B., Christensen, B., Fulthorpe, C., Gallagher, S. J., and Henderiks, J.: Timing and Pacing of Indonesian Throughflow Restriction and Its Connection to Late Pliocene Climate Shifts, *Paleoceanography and Paleoclimatology*, 34, 635–657, <https://doi.org/10.1029/2018PA003512>, 2019.
- Aze, T., Ezard, T. H. G., Purvis, A., Coxall, H. K., Stewart, D. R. M., Wade, B. S., and Pearson, P. N.: A phylogeny of Cenozoic macroperforate planktonic foraminifera from fossil data, *Biol. Rev.*, 86, 900–927, <https://doi.org/10.1111/j.1469-185X.2011.00178.x>, 2011.
- Backman, J. and Shackleton, N. J.: Quantitative biochronology of Pliocene and early Pleistocene calcareous nannofossils from the Atlantic, Indian and Pacific oceans, *Mar. Micropaleontol.*, 8, 141–170, [https://doi.org/10.1016/0377-8398\(83\)90009-9](https://doi.org/10.1016/0377-8398(83)90009-9), 1983.
- Backman, J., Raffi, I., Rio, D., Fornaciari, E., and Pälike, H.: Biozonation and biochronology of Miocene through Pleistocene calcareous nannofossils from low and middle latitudes, *Newsl. Stratigr.*, 45, 221–244, <https://doi.org/10.1127/0078-0421/2012/0022>, 2012.
- Bard, E. and Rickaby, R. E. M.: Migration of the subtropical front as a modulator of glacial climate, *Nature*, 460, 380–393, <https://doi.org/10.1038/nature08189>, 2009.
- Bé, A. W. H. and Duplessy, J.-C.: Subtropical Convergence Fluctuations and Quaternary Climates in the Middle Latitudes of the Indian Ocean, *Science*, 194, 419–422, <https://doi.org/10.1126/science.194.4263.419>, 1976.
- Bé, A. W. H. and Tolderlund, D. S.: Distribution and ecology of living planktonic foraminifera in surface waters of the Atlantic and Indian oceans, in: *The micropalaeontology of the oceans*, edited by: Funnell, B. H. and Riedel, W. R., London, Cambridge Univ. Press, 105–149, ISBN 0521076420, 1971.
- Becquey, S. and Gersonde, R.: Past hydrographic and climatic changes in the Subantarctic Zone of the South Atlantic – The Pleistocene record from ODP Site 1090, *Palaeogeogr. Palaeoclimatol.*, 182, 221–239, [https://doi.org/10.1016/S0031-0182\(01\)00497-7](https://doi.org/10.1016/S0031-0182(01)00497-7), 2002.
- Berger, W. H. and Jansen, E.: Mid-Pleistocene Climate Shift – The Nansen Connection, in: *The Polar Oceans and Their Role in Shaping the Global Environment*, edited by: Johannessen, O. M., Muench, R. D., and Overland, J. E., <https://doi.org/10.1029/GM085p0295>, 1994.
- Biastoch, A., Boning, C. W., and Lutjeharms, J. R. E.: Agulhas leakage dynamics affects decadal variability in Atlantic overturning circulation, *Nature*, 456, 489–492, <https://doi.org/10.1038/nature07426>, 2008.
- Billups, K., Hudson, C., Kunz, H., and Rew, I.: Exploring *Globorotalia truncatulinoides* coiling ratios as a proxy for subtropical gyre dynamics in the northwestern Atlantic Ocean during late Pleistocene Ice Ages, *Paleoceanography*, 31, 553–563, <https://doi.org/10.1002/2016PA002927>, 2016.
- Bjerknes, J.: Atmospheric Teleconnections from the Equatorial Pacific, *J. Phys. Oceanogr.*, 97, 163–172, [https://doi.org/10.1175/1520-0493\(1969\)097<0163:ATFTEP>2.3.CO;2](https://doi.org/10.1175/1520-0493(1969)097<0163:ATFTEP>2.3.CO;2), 1969.
- Blow, W. H.: Late Middle Eocene to Recent Planktonic Foraminiferal Biostratigraphy, in: *Proceedings of the 1st International Conference on Planktonic Microfossils*, edited by: Brönnimann, P. and Renz, H. H., Geneva, 1, 199–422, 1969.
- Bolli, H. M. and Saunders, J. B.: Cretaceous Planktic Foraminifera, in: *Plankton Stratigraphy*, edited by: Bolli, H. M., Saunders, J. B., and Perch Nielsen, K., Cambridge: Cambridge University Press, 17–86, ISBN 0 521 23576 6, 1985.
- Bown, P. and Dunkley-Jones, T.: Calcareous nannofossils from the Paleogene equatorial Pacific (IODP Expedition 320 Sites U1331–1334), *Journal of Nannoplankton Research*, 32, 3–51, 2012.
- Bown, P., and Young, J.: Techniques, in: *Calcareous Nannofossil Biostratigraphy*, edited by: Bown, P. R., Chapman and Hall, Cambridge, 16–28, ISBN 0 412 78970 1, 1998.
- Boyd, A. J. and Thomas, R. M.: A southward intrusion of equatorial water off northern and central Namibia in March 1984, *Trop. Ocean-Atmos. Newsl.*, 27, 16–17, 1984.
- Boyd, A. J., Salat, J., and Masó, M.: The seasonal intrusion of relatively saline water on the shelf off northern and central Namibia, in: *The Benguela and Comparable Ecosystems*, edited by: Payne, A. I. L., Gulland, J. A., and Brink, K. H., *S. Afr. J. Marine Sci.*, 5, 107–120, 1987.
- Boyer, D. C., Boyer, H. J., Fossen, I., and Kreiner, A.: Changes in abundance of the northern Benguela sardine stock during the decade 1990–2000, with comments on the relative importance of fishing and the environment, *S. Afr. J. Marine Sci.*, 23, 67–84, <https://doi.org/10.2989/025776101784528854>, 2001.
- Bremner, J. M.: Biogenic Sediments on the South West African (Namibian) Continental Margin, in: *Coastal Upwelling: Its Sediment Record. Part B: Sedimentary Record of Ancient Coastal Upwelling*, edited by: Thiede, J. and Suess, E., Plenum Press, New York, 73–103, ISBN 0-306-41352-3, 1983.
- Brummer, G.-J. A. and Kroon, D.: Genetically controlled planktonic foraminiferal coiling ratios as tracers of past ocean dynamics, in *Planktonic Foraminifera as Tracers of Ocean-Climate History*, edited by: Brummer, G.-J. A. and Kroon, D., 293–298, Free Univ. Press, Amsterdam, 1988.
- Bylinskaya, M. E.: Range and stratigraphic significance of the *Globorotalia crassaformis* plexus, *J. Iber. Geol.*, 31, 51–63, 2004.
- Caley, T., Giraudeau, J., Malaize, B., Rossignol, L., and Pierre, C.: Agulhas leakage as a key process in the modes of Quaternary climate changes, *P. Natl. Acad. Sci. USA*, 109, 6835–6839, <https://doi.org/10.1073/pnas.1115545109>, 2012.
- Caley, T., Peeters, F. J. C., Biastoch, A., Rossignol, L., Van Sebille, E., Durgadoo, J., Malaizé, B., Giraudeau, J., Arthur, K., and Zahn, R.: Quantitative estimate of the paleo-Agulhas leakage, *Geophys. Res. Lett.*, 41, 1238–1246, <https://doi.org/10.1002/2014GL059278>, 2014.
- Chaisson, W. P. and Leckie, R. M.: High-resolution Neogene planktonic foraminifer biostratigraphy of Site 806, Ontog Java Plateau (Western Equatorial Pacific), in: *Proceedings ODP, Scientific Results 130*, College Station, TX (Ocean Drilling Program), edited by: Kroenke, L. W., Berger, W. H., Janecek, T. R., Backman, J., Bassinot, F., Corfield, R. M., Delaney, M. L., Hagen, R., Jansen, E., Kriesek, L. A., Lange, C., Leckie, R. M., Lind, I. L., Lyle, M. W., Mahoney, J. J., Marsters, J. C., Mayer, L., Mosher, D. C., Musgrave, R., Prentice, M. L., Resig, J. M., Schmidt, H., Stax, R., Storey, M., Takahashi, K.,

- Takayama, T., Tarduno, J. A., Wilkens, R. H., and Wu, G., 137–178, <https://doi.org/10.2973/odp.proc.sr.130.010.1993>, 1993.
- Chaisson, W. P. and Ravelo, A. C.: Changes in upper water-column structure at Site 925, late Miocene–Pleistocene: planktonic foraminifer assemblage and isotopic evidence, in: Proc. ODP, Sci. Results, College Station, TX., edited by: Shackleton, N. J., Curry, W. B., Richter, C., and Bralower, T. J., 154, 255–268, <https://doi.org/10.2973/odp.proc.sr.154.105.1997>, 1997.
- Christensen, B. A. and Giraudeau, J.: Neogene and Quaternary evolution of the Benguela upwelling system, *Mar. Geol.*, 180, 1–2, [https://doi.org/10.1016/S0025-3227\(01\)00202-X](https://doi.org/10.1016/S0025-3227(01)00202-X), 2002.
- Connary, S. D.: Investigations of the Walvis Ridge and environs, PhD thesis, Columbia University, New York, 228 pp., <https://digital.unam.edu.na/handle/11070.1/4199> (last access: 17 February 2024), 1972.
- Curry, W. B., Thunell, R. C., and Honjo, S.: Seasonal changes in the isotopic composition of planktonic foraminifera collected in Panama Basin sediment traps, *Earth Planet. Sc. Lett.*, 64, 33–43, [https://doi.org/10.1016/0012-821x\(83\)90050-x](https://doi.org/10.1016/0012-821x(83)90050-x), 1983.
- Darling, K. F., Kucera, M., Kroon, D., and Wade, C. M.: A resolution for the coiling direction paradox in *Neoglobobulimina papyroderma*, *Paleoceanography*, 21, PA2011, <https://doi.org/10.1029/2005PA001189>, 2006.
- Del Gaudio, A. V., Piller, W. E., Auer, G., and Kurz, W.: Foraminifera assemblages from Fantangisña serpentinite mud seamount in the NW Pacific Ocean during the Pleistocene (IODP Expedition 366), *J. Quaternary Sci.*, 38, 1103–1127, <https://doi.org/10.1002/jqs.3532>, 2023.
- Del Gaudio, A. V., Avery, A., Auer, G., Piller, W. E., and Kurz, W.: Planktonic foraminiferal assemblages of IODP Site U1575, PANGAEA [data set], <https://doi.org/10.1594/PANGAEA.965686>, 2024a.
- Del Gaudio, A. V., Avery, A., Auer, G., Piller, W. E., and Kurz, W.: Planktonic foraminiferal assemblages of IODP Site U1576, PANGAEA [data set], <https://doi.org/10.1594/PANGAEA.965703>, 2024b.
- Detrick, R. S. and Watts, A. B.: An Analysis of Isostasy in the World's Oceans 3. Aseismic Ridges, *J. Geophys. Res.*, 84, 3637–3653, <https://doi.org/10.1029/JB084iB07p03637>, 1979.
- Dickson, A. J., Leng, M. J., Maslin, M. A., Sloane, H. J., Green, J., Bendle, J. A., McClymont, E., and Pancost, R. D.: Atlantic overturning circulation and Agulhas leakage influences on Southeast Atlantic upper ocean hydrography during marine isotope stage 11, *Paleoceanography*, 25, PA3208, <https://doi.org/10.1029/2009PA001830>, 2010.
- Diekmann, B. and Kuhn, G.: Sedimentary record of the mid-Pleistocene climate transition in the southeastern South Atlantic (ODP Site 1090), *Palaeogeogr. Palaeoclimatol.*, 182, 241–258, [https://doi.org/10.1016/S0031-0182\(01\)00498-9](https://doi.org/10.1016/S0031-0182(01)00498-9), 2002.
- Diester-Haass, L.: Sea level changes, carbonate dissolution and history of the Benguela Current in the Oligocene–Miocene off Southwest Africa (DSDP Site 362, Leg 40), *Mar. Geol.*, 79, 213–242, [https://doi.org/10.1016/0025-3227\(88\)90040-0](https://doi.org/10.1016/0025-3227(88)90040-0), 1988.
- Drouin, K. L., Lozier, M. S., and Johns, W. E.: Variability and trends of the South Atlantic subtropical gyre, *J. Geophys. Res.–Oceans*, 126, e2020JC016405, <https://doi.org/10.1029/2020JC016405>, 2021.
- Etourneau, J., Martinez, P., Blanz, T., and Schneider, R.: Pliocene–Pleistocene variability of upwelling activity, productivity, and nutrient cycling in the Benguela region, *Geology*, 37, 871–874, <https://doi.org/10.1130/g25733a.1>, 2009.
- Etourneau, J., Schneider, R., Blanz, T., and Martinez, P.: Intensification of the Walker and Hadley atmospheric circulations during the Pliocene–Pleistocene climate transition, *Earth. Planet. Sc. Lett.*, 297, 103–110, <https://doi.org/10.1016/j.epsl.2010.06.010>, 2010.
- Fairbanks, R. G., Sverdrup, M., Free, R., Wiebe, H. P., and Bé, A. W. H.: Vertical distribution and isotopic fractionation of living planktonic foraminifera from the Panama Basin, *Nature*, 298, 841–844, <https://doi.org/10.1038/298841a0>, 1982.
- Fairhead, J. D. and Wilson, M.: Plate tectonic processes in the South Atlantic Ocean: Do we need deep mantle plumes?, in: Plates, plumes and paradigms, edited by: Foulger, G. R., Natland, J. H., Presnall, D. C., and Anderson D. L., The Geological Society of America, 388, 537–553, <https://doi.org/10.1130/0-8137-2388-4.537>, 2005.
- Fedorov, A., Brierley, C., and Emanuel, K.: Tropical cyclones and permanent El Niño in the early Pliocene epoch, *Nature*, 463, 1066–1070, <https://doi.org/10.1038/nature08831>, 2010.
- Feldmeijer, W., Metcalfe, B., Brummer, G., and Ganssen, G.: Reconstructing the depth of the permanent thermocline through the morphology and geochemistry of the deep dwelling planktonic foraminifer *Globorotalia truncatulinoides*, *Paleoceanography*, 30, 1–22, <https://doi.org/10.1002/2014PA002687>, 2014.
- Fine, R. A., Warner, M. J., and Weiss, R. F.: Water mass modification at the Agulhas. Retroflexion: chlorofluoromethane studies, *Deep-Sea Res.*, 35, 311–332, 1988.
- Foulger, G.: The “plate” model for the genesis of melting anomalies, in: Plates, Plumes and Planetary Processes, edited by: Foulger, G. and Jurdy, D. M., The Geological Society of America, 430, 28 pp., [https://doi.org/10.1130/2007.2430\(01\)](https://doi.org/10.1130/2007.2430(01)), 2007.
- Franzese, A. M., Hemming, S. R., Goldstein, S. L., and Anderson, R. F.: Reduced Agulhas leakage during the Last Glacial Maximum inferred from an integrated provenance and flux study, *Earth. Planet. Sc. Lett.*, 250, 72–88, <https://doi.org/10.1016/j.epsl.2006.07.002>, 2006.
- Friesenhagen, T.: Test-size evolution of the planktonic foraminifer *Globorotalia menardii* in the eastern tropical Atlantic since the Late Miocene, *Biogeosciences*, 19, 777–805, <https://doi.org/10.5194/bg-19-777-2022>, 2022.
- Gammelsrød, T., Bartholomae, C. H., Boyer, D. C., Filipe, V. L. L., and O’Toole, M. J.: Intrusion of warm surface water along the Angolan–Namibian coast in February–March 1995: The 1995 Benguela Niño, *S. Afr. J. Marine Sci.*, 19, 41–56, <https://doi.org/10.2989/025776198784126719>, 1998.
- Garzoli, S. L. and Gordon, A. L.: Origins and variability of the Benguela Current, *J. Geophys. Res.*, 101, 897–906, <https://doi.org/10.1029/95JC03221>, 1996.
- Garzoli, S. L., Gordon, A. L., Kamenkovich, V., Pillsbury, D., and Duncombe-Rae, C.: Variability and sources of the southwestern Atlantic circulation, *J. Mar. Res.*, 54, 1039–1071, <https://doi.org/10.1357/0022240963213763>, 1996.
- Giraudeau, J.: Distribution of Recent nannofossils beneath the Benguela system: Southwest African continental margin, *Mar. Geol.*, 108, 219–237, [https://doi.org/10.1016/0025-3227\(92\)90174-G](https://doi.org/10.1016/0025-3227(92)90174-G), 1992.
- Giraudeau, J.: Planktonic foraminiferal assemblages in surface sediments from the southwest African continental mar-

- gin, *Mar. Geol.*, 110, 47–62, [https://doi.org/10.1016/0025-3227\(93\)90104-4](https://doi.org/10.1016/0025-3227(93)90104-4), 1993.
- Gordon, W. A.: Marine Life and Ocean Surface Currents in the Cretaceous, *J. Geol.*, 81, 269–284, <https://www.jstor.org/stable/30084824> (last access: 25 February 2024), 1973.
- Gradstein, F. M., Ogg, J. G., Schmitz, M. D., and Ogg, G. M.: The Geologic Time Scale 2020, Elsevier, 2, 565–1357, ISBN 978-0-12-824363-3, 2020.
- Hammer, Ø., Harper, D. A. T., and Ryan, P. D.: PAST – Palaeontological Statistics, Natural History Museum [code], <https://www.nhm.uio.no/english/research/resources/past/>, 2001.
- Haq, B. U. and Lohmann, G. P.: Early Cenozoic calcareous nannoplankton biogeography of the Atlantic Ocean, *Mar. Micropaleontol.*, 1, 119–194, [https://doi.org/10.1016/0377-8398\(76\)90008-6](https://doi.org/10.1016/0377-8398(76)90008-6), 1976.
- Haynes, J. R.: Foraminifera. New York, New York: John Wiley and Sons, 433 pp., ISBN 978-1-349-05397-1, 1981.
- Head, M. J. and Gibbard, P. L.: Early-Middle Pleistocene transitions: Linking terrestrial and marine realms, *Quatern. Int.*, 389, 7–46, <https://doi.org/10.1016/j.quaint.2015.09.042>, 2015.
- Hemleben, C., Spindler, M., Breiting, I., and Ott, R.: Morphological and physiological responses of *Globigerinoides sacculifer* (Brady) under varying laboratory conditions, *Mar. Micropaleontol.*, 12, 305–324, [https://doi.org/10.1016/0377-8398\(87\)90025-9](https://doi.org/10.1016/0377-8398(87)90025-9), 1987.
- Herbert, R. S.: Late Holocene climatic change: the Little Ice Age and El Niño from planktonic Foraminifera in sediments off Walvis Bay, South West Africa, Joint Geological Survey/University of Cape Town Marine Geoscience Group, 18, 45 pp., <https://open.uct.ac.za/handle/11427/6568> (last access: 16 January 2024), 1987.
- Herbert, T. D.: The Mid-Pleistocene Climate Transition. *Annu. Rev. Earth Pl. Sc.*, 51, 389–418, <https://doi.org/10.1146/annurev-earth-032320-104209>, 2023.
- Herman, Y.: *Globorotalia truncatulinoides*: a Palaeoceanographic Indicator, *Nature*, 238, 394–396, <https://doi.org/10.1038/238394a0>, 1972.
- Hisard, P.: Observation de réponses de type “El Niño” dans l’Atlantique tropical oriental-Golfe de Guinée, *Oceanol. Acta*, 3, 69–78, <https://archimer.ifremer.fr/doc/00122/23296/21123.pdf>, 1980.
- Hodell, D. A., Charles, C. D., and Ninnemann, U. S.: Comparison of interglacial stages in the South Atlantic sector of the southern ocean for the past 450 kyr: implications for Marine Isotope Stage (MIS) 11, *Global Planet. Change*, 24, 7–26, [https://doi.org/10.1016/S0921-8181\(99\)00069-7](https://doi.org/10.1016/S0921-8181(99)00069-7), 2000.
- Homrighausen, S., Hoernle, K., Hauff, F., Wartho, J.-A., van den Bogaard, P., and Garbe-Schönberg, D.: New age and geochemical data from the Walvis Ridge: The temporal and spatial diversity of South Atlantic intraplate volcanism and its possible origin, *Geochim. Cosmochim. Ac.*, 245, 16–34, <https://doi.org/10.1016/j.gca.2018.09.002>, 2019.
- Hoernle, K., Werner, R., Morgan, J. P., Garbe-Schönberg, D., Bryce, J., and Mrazek, J.: Existence of complex spatial zonation in the Galápagos plume, *Geology*, 28, 435–438, [https://doi.org/10.1130/0091-7613\(2000\)28<435:EOCSZI>2.0.CO;2](https://doi.org/10.1130/0091-7613(2000)28<435:EOCSZI>2.0.CO;2), 2000.
- Hoernle, K., Rohde, J., Hauff, F., Garbe-Schönberg, D., Homrighausen, S., Werner, R., and Morgan, J. P.: How and when plume zonation appeared during the 132 Myr evolution of the Tristan Hotspot, *Nat. Commun.*, 6, 7799, <https://doi.org/10.1038/ncomms8799>, 2015.
- Humphris, S. E. and Thompson, G.: A geochemical study of rocks from the Walvis Ridge, South Atlantic, *Chem. Geol.*, 36, 253–274, [https://doi.org/10.1016/0009-2541\(82\)90051-1](https://doi.org/10.1016/0009-2541(82)90051-1), 1982.
- Hutchings, L., van der Lingen, C. D., Shannon, L. J., Crawford, R. J. M., Verheye, H. M. S., Bartholomae, C. H., van der Plas, A. K., Louw, D., Kreiner, A., Ostrowski, M., Fidel, Q., Barlow, R. G., Lamont, T., Coetzee, J., Shillington, F., Veitch, J., Currie, J. C., and Monteiro, P. M. S.: The Benguela Current: An ecosystem of four components, *Prog. Oceanogr.*, 83, 15–32, <https://doi.org/10.1016/j.pocean.2009.07.046>, 2009.
- Illig, S. and Bachèlery, M. L.: The 2021 Atlantic Niño and Benguela Niño Events: external forcings and air–sea interactions, *Clim. Dynam.*, 62, 679–702, <https://doi.org/10.1007/s00382-023-06934-0>, 2024.
- Illig, S., Dewitte, B., Ayoub, N., du Penhoat, Y., Reverdin, G., Mey, P. D., Bonjean, F., and Lagerloef, G. S. E.: Interannual long equatorial waves in the tropical Atlantic from a high-resolution ocean general circulation model experiment in 1981–2000, *J. Geophys. Res.*, 109, C02022, <https://doi.org/10.1029/2003JC001771>, 2004.
- Imbol Koungue, R. A. and Brandt, P.: Impact of intraseasonal waves on Angolan warm and cold events, *J. Geophys. Res.-Oceans*, 126, e2020JC017088, <https://doi.org/10.1029/2020JC017088>, 2021.
- Imbol Koungue, R. A., Rouault, M., Illig, S., Brandt, P., and Jouanno, J.: Benguela Niños and Benguela Niñas in forced ocean simulation from 1958 to 2015, *J. Geophys. Res.-Oceans*, 124, 5923–5951, <https://doi.org/10.1029/2019JC015013>, 2019.
- Jayan, A. K., Sijinkumar, A. V., and Nagender Nath, B.: Paleocceanographic significance of *Globigerinoides ruber* (white) morphotypes from the Andaman Sea, *Mar. Micropaleontol.*, 165, 101996, <https://doi.org/10.1016/j.marmicro.2021.101996>, 2021.
- Jansen, J. H. F., Ufkes, E., and Schneider, R. R.: Late Quaternary movements of the Angola-Benguela Front, SE Atlantic, and implications for advection in the equatorial Ocean, in *The South Atlantic*, edited by: Wefer, G., Berger, W. H., Siedler, G., and Webb, D. J., Springer, New York, 553–575, ISBN 978-3-642-80355-0, 1996.
- Kaboth-Bahr, S. and Mudelsee, M.: The multifaceted history of the Walker Circulation during the Pliocene-Pleistocene, *Quaternary Sci. Rev.*, 286, 107529, <https://doi.org/10.1016/j.quascirev.2022.107529>, 2022.
- Keany, J. and Kennett, J. P.: Pliocene-Early Pleistocene Paleoclimatic History Recorded in Antarctic-Subantarctic Deep-Sea Cores, *Deep-Sea Res.*, 19, 529–548, 1972.
- Kennet, J. P. and Srinivasan, M. S.: Neogene planktonic foraminifera: A Phylogenetic Atlas. Stroudsburg: Hutchinson Ross publishing company, p. 265, ISBN 0-87933-070-8, 1983.
- Klein, P. and Lapeyre, G.: The Oceanic Vertical Pump Induced by Mesoscale and Submesoscale Turbulence, *Annu. Rev. Mar. Sci.*, 1, 351–375, <https://doi.org/10.1146/annurev.marine.010908.163704>, 2009.
- Kopte, R., Brandt, P., Dengler, M., Tchupalanga, P. C. M., Macuéria, M., and Ostrowski, M.: The Angola Current: Flow and hydrographic characteristics as observed

- at 11°S, *J. Geophys. Res.-Oceans*, 122, 1177–1189, <https://doi.org/10.1002/2016JC012374>, 2017.
- Lam, A. R. and Leckie, R. M.: Late Neogene and Quaternary diversity and taxonomy of subtropical to temperate planktic foraminifera across the Kuroshio Current Extension, northwest Pacific Ocean, *Micropaleontology*, 114, 19–35, <https://doi.org/10.47894/mpal.66.3.01>, 2020.
- Little, M. G., Schneider, R., Kroon, D., Price, B., Bickert, T., and Wefer, G.: Rapid palaeoceanographic changes in the Benguela Upwelling System for the last 160,000 years as indicated by abundances of planktonic foraminifera, *Palaeogeogr. Palaeoclimatol.*, 130, 135–161, [https://doi.org/10.1016/S0031-0182\(96\)00136-8](https://doi.org/10.1016/S0031-0182(96)00136-8), 1997.
- Loeblich Jr., A. R. and Tappan, H.: Foraminifera of the Sahul shelf and Timor Sea. Cushman Foundation for Foraminiferal Research, Special publication, 31, 661 pp., 1994.
- Lohmann, G. P. and Schweitzer, P. N.: *Globorotalia truncatulinoides*' Growth and chemistry as probes of the past thermocline: 1. Shell size, *Paleoceanography*, 5, 55–75, <https://doi.org/10.1029/PA005i001p00055>, 1990.
- Lombard, F., Labeyrie, L., Michel, E., Bopp, L., Cortijo, E., Retailliau, S., Howa, H., and Jorissen, F.: Modelling planktic foraminifer growth and distribution using an ecophysiological multi-species approach, *Biogeosciences*, 8, 853–873, <https://doi.org/10.5194/bg-8-853-2011>, 2011.
- Lutjeharms, J. R. E.: Satellite Studies of the South Atlantic Upwelling System, in: *Oceanography from Space*, edited by: Gower, J. F. R., *Mar. Sci.*, 13, Springer, Boston, MA, https://doi.org/10.1007/978-1-4613-3315-9_24, 1981.
- Lutjeharms, J. R. E. and Meeuwis, J. M.: The extent and variability of South-East Atlantic upwelling, *S. Afr. J. Marine Sci.*, 5, 51–62, <https://doi.org/10.2989/025776187784522621>, 1987.
- Lutjeharms, J. R. E. and Stockton, P. L.: Kinematics of the upwelling front off southern Africa, *S. Afr. J. Marine Sci.*, 5, 35–49, <https://doi.org/10.2989/025776187784522612>, 1987.
- Maiorano, P. and Marino, M.: Calcareous nannofossil bioevents and environmental control on temporal and spatial patterns at the early–middle Pleistocene, *Mar. Micropaleontol.*, 53, 405–422, <https://doi.org/10.1016/j.marmicro.2004.08.003>, 2004.
- Manabe, S. and Broccoli, A. J.: The influence of continental ice sheets on the climate of an ice age, *J. Geophys. Res.*, 90, 2167–2190, <https://doi.org/10.1029/JD090iD01p02167>, 1985.
- Marino, G., Zahn, R., Ziegler, M., Purcell, C., Knorr, G., Hall, I. R., Ziveri, P., and Elderfield, H.: Agulhas salt-leakage oscillations during abrupt climate changes of the late Pleistocene, *Paleoceanography*, 28, 599–606, <https://doi.org/10.1002/palo.20038>, 2013.
- Marlow, J. R., Lange, C. B., Wefer, G., and Rosell-Mele, A.: Upwelling intensification as part of the Pliocene–Pleistocene climate transition, *Science*, 290, 2288–2291, <https://doi.org/10.1126/science.290.5500.2288>, 2000.
- Martinez-Garcia, A., Rosell-Mele, A., McClymont, E. L., Gersonde, R., and Haug, G. H.: Subpolar link to the emergence of the modern equatorial Pacific cold tongue, *Science*, 328, 1550–1553, <https://doi.org/10.1126/science.1184480>, 2010.
- Martínez-Méndez, G., Zahn, R., Hall, R., Pena, L. D., and Cacho, I.: 345,000-year-long multi-proxy records off South Africa document variable contributions of northern versus southern component water to the deep South Atlantic, *Earth. Planet. Sc. Lett.*, 267, 309–321, <https://doi.org/10.1016/j.epsl.2007.11.050>, 2008.
- McClymont, E. L., Rosell-Melé, A., Giraudeau, J., Pierre, C., and Lloyd, J. M.: Alkenone and coccolith records of the mid-Pleistocene in the south-east Atlantic: implications for the U_{37}^K index and South African climate, *Quaternary Sci. Rev.*, 24, 1559–1572, <https://doi.org/10.1016/j.quascirev.2004.06.024>, 2005.
- McIntyre, A., Ruddiman, W. F., Karlin, K., and Mix, A. C.: Surface water response of the equatorial Atlantic Ocean to orbital forcing, *Paleoceanography*, 4, 19–55, <https://doi.org/10.1029/PA004i001p00019>, 1989.
- Mohrholz, V., Bartholomae, C. H., van der Plas, A. K., and Lass, H. U.: The seasonal variability of the northern Benguela undercurrent and its relation to the oxygen budget on the shelf, *Cont. Shelf Res.*, 28, 424–441, <https://doi.org/10.1016/j.csr.2007.10.001>, 2008.
- Monteiro, P. M. S. and van der Plas, A. K.: Low oxygen water (LOW) variability in the Benguela system: Key processes and forcing scales relevant to forecasting, *Lar. Mar. Ecosyst.*, 14, 71–90, [https://doi.org/10.1016/S1570-0461\(06\)80010-8](https://doi.org/10.1016/S1570-0461(06)80010-8), 2006.
- Morgan, W. J.: Convection Plumes in the Lower Mantle, *Nature*, 230, 42–43, <https://doi.org/10.1038/230042a0>, 1971.
- Oberhänsli, H., Bénier, C., Meinecke, G., Schmidt, H., Schneider, R., and Wefer, G.: Planktonic foraminifera as tracers of ocean currents in the eastern South Atlantic, *Paleoceanography*, 7, 607–632, <https://doi.org/10.1029/92PA01236>, 1992.
- Olson, D. B. and Evans, R. H.: Rings of the Agulhas current, *Deep-Sea Res.*, 33, 27–42, [https://doi.org/10.1016/0198-0149\(86\)90106-8](https://doi.org/10.1016/0198-0149(86)90106-8), 1986.
- Peeters, F. J. C., Acheson, R., Brummer, G.-J. A., de Ruijter, W. P. M., Schneider, R. R., Ganssen, G. M., Ufkes, E., and Kroon, D.: Vigorous exchange between the Indian and Atlantic oceans at the end of the past five glacial periods, *Nature*, 430, 661–665, <https://doi.org/10.1038/nature02785>, 2004.
- Perch-Nielsen, K.: Mesozoic calcareous nannofossils, in: *Plankton Stratigraphy*, edited by: Bolli, H. M., Saunders, J. B., and Perch-Nielsen, K., Vol. 1, Cambridge University Press, Cambridge, 329–426, ISBN 0 521 36719, 1985a.
- Perch-Nielsen, K.: Cenozoic calcareous nannofossils, in: *Plankton Stratigraphy*, edited by: Bolli, H. M., Saunders, J. B., and Perch-Nielsen, K., Vol. 1, Cambridge University Press, Cambridge, 427–554, ISBN 0 521 36719, 1985b.
- Petrick, B., McClymont, E. L., Littler, K., Rosell-Melé, A., Clarkson, M. O., Maslin, M., Röhl, U., Shevenell, A. E., and Pancost, R. D.: Oceanographic and climatic evolution of the southeastern subtropical Atlantic over the last 3.5 Ma, *Earth. Planet. Sc. Lett.*, 492, 12–21, <https://doi.org/10.1016/j.epsl.2018.03.054>, 2018.
- Petrick, B. F., McClymont, E. L., Marret, F., and van der Meer, M. T. J.: Changing surface water conditions for the last 500 ka in the Southeast Atlantic: Implications for variable influences of Agulhas leakage and Benguela upwelling, *Paleoceanography*, 30, 1153–1167, <https://doi.org/10.1002/2015PA002787>, 2015.
- Philander, S. G. H.: *El Niño, La Niña and the Southern Oscillation*, Academic Press, Cambridge, 293 pp., ISBN 978-0125532358, 1990.
- Pickard, G. L. and Emery, W. J.: *Descriptive Physical Oceanography*, Pergamon Press, New York, 320 pp., ISBN 0-08-037953-2, 1991.

- Pinho, T. M. L., Chiessi, C. M., Portilho-Ramos, R. C., Campos, M. C., Crivellari, S., Nascimento, R. A., Albuquerque, A. L. S., Bahr, A., and Multiza, S.: Meridional changes in the South Atlantic Subtropical Gyre during Heinrich Stadials, *Sci. Rep.*, 11, 9419, <https://doi.org/10.1038/s41598-021-88817-0>, 2021.
- Postuma, J. A.: Manual of planktonic foraminifera, 1st edn., Elsevier Publishing Company, p. 422, ISBN 0-444-40909-2, 1971.
- Qiu, B. and Chen, S.: Interannual-to-decadal variability in the bifurcation of the North Equatorial Current off the Philippines, *J. Phys. Oceanogr.*, 40, 213–225, <https://doi.org/10.1175/2010JPO4462.1>, 2010.
- Raffi, I.: Revision of the early-middle Pleistocene calcareous nannofossil biochronology (1.75–0.85 Ma), *Mar. Micropaleontol.*, 45, 25–55, 2002.
- Raffi, I., Rio, D., d’Atri, A., Fornaciari, E., and Rocchetti, S.: Quantitative Distribution Patterns and Biomagnetostratigraphy of Middle and Late Miocene Calcareous Nannofossils from Equatorial Indian and Pacific Oceans (Legs 115, 130, and 138), in: *Proc. ODP, Sci. Results*, College Station, TX, edited by: Pisias, N. G., Mayer, L. A., Janecek, T. R., Palmer-Julson, A., and van Andel, T. H., 138, 479–502, <https://doi.org/10.2973/odp.proc.sr.138.125.1995>, 1995.
- Raffi, I., Backman, J., Fornaciari, E., Päläike, H., Rio, D., Lourens, L., and Hilgen, F.: A review of calcareous nannofossil astrobiochronology encompassing the past 25 million years, *Quaternary Sci. Rev.*, 25, 3113–3137, <https://doi.org/10.1016/j.quascirev.2006.07.007>, 2006.
- Rögl, F.: The evolution of the Globorotalia truncatulinoides and Globorotalia crassaformis group in the Pliocene and Pleistocene of the Timor Trough, DSDP Leg 27, Site 262, in: *Initial Reports of the DSDP 27*, Washington (U. S. Govt. Printing Office), edited by: Veevers, J. J., Heirtzler, J. R., Bolli, H. M., Carter, A. N., Cook, P. J., Krasheninnikov, V., McKnight, B. K., Proto Decima, F., Renz, G. W., Robinson, P. T., Rucker, K., and Thayer Jr., P. A., 743–767, <https://doi.org/10.2973/dsdp.proc.27.137.1974>, 1974.
- Rosell-Melé, A., Martínez-García, A., and McClymont, E. L.: Persistent warmth across the Benguela upwelling system during the Pliocene epoch, *Earth Planet. Sc. Lett.*, 386, 10–20, <https://doi.org/10.1016/j.epsl.2013.10.041>, 2014.
- Rouault, M. and Tomety, F. S.: Impact of El Niño–Southern Oscillation on the Benguela Upwelling, *J. Phys. Oceanogr.*, 52, 2573–2587, <https://doi.org/10.1175/JPO-D-21-0219.1>, 2022.
- Rouault, M., Illig, S., Bartholomae, C., Reason, C. J. C., and Bentamy, A.: Propagation and origin of warm anomalies in the Angola Benguela upwelling system in 2001, *J. Marine Syst.*, 68, 473–488, <https://doi.org/10.1016/j.jmarsys.2006.11.010>, 2007.
- Sager, W., Hoernle, K., and Petronotis, K.: Expedition 391 Scientific Prospectus: Walvis Ridge Hotspot. College Station, TX, International Ocean Discovery Program, <https://doi.org/10.14379/iodp.sp.391.2020>, 2020.
- Sager, W., Hoernle, K., Höfig, T. W., and the Expedition 391 Scientists: Expedition 391 Preliminary Report: Walvis Ridge Hotspot, College Station, TX, International Ocean Discovery Program, <https://doi.org/10.14379/iodp.pr.391.2022>, 2022.
- Sager, W., Hoernle, K., Höfig, T. W., Avery, A. J., Bhutani, R., Buchs, D. M., Carvallo, C. A., Class, C., Dai, Y., Dalla Valle, G., Del Gaudio, A. V., Fielding, S., Gastra, K. M., Han, S., Homrighausen, S., Kubota, Y., Li, C.-F., Nelson, W. R., Petrou, E., Potter, K. E., Pujatti, S., Scholpp, J., Shervais, J. W., Thoram, S., Tikoo-Schantz, S. M., Tshiningayawme, M., Wang, X.-J., and Widdowson, M.: Expedition 391 methods, in: *Proceedings of the International Ocean Discovery Program, 391*, College Station, TX, edited by: Sager, W., Hoernle, K., Höfig, T. W., Blum, P., and the Expedition 391 Scientists, Walvis Ridge Hotspot, <https://doi.org/10.14379/iodp.proc.391.102.2023>, 2023.
- Salzmann, U., Williams, M., Haywood, A. M., Johnson, A. L. A., Kender, S., and Zalasiewicz, J.: Climate and environment of a Pliocene warm world, *Palaeogeogr. Palaeoclimatol.*, 309, 1–8, <https://doi.org/10.1016/j.palaeo.2011.05.044>, 2011.
- Sato, T., Kameo, K., and Takayama, T.: Coccolith biostratigraphy of the Arabian Sea, in: *Proc. ODP, Sci. Results*, College Station, TX, edited by: Prell, W. L., Niituma, M., Emeis, K.-C., Al-Sulaiman, Z. K., Al-Tobba, A. N. K., Anderson, D. M., Barnes, R. O., Bilak, R. A., Bloemendal, J., Bray, C. J., Busch, W. H., Clemens, S. C., de Menocal, P., Debrabant, P., Hayashida, A., J. Hermelin, O. R., Jarrard, R. D., Kriesek, L. A., Kroon, D., Murray, D. W., Nigrini, C. A., Pedersen, T. F., Ricken, W., Shimmield, G.B., Spaulding, S. A., Takayama, T., Lo ten Haven, H., and Weedon, G. P., 117, 37–54, <https://doi.org/10.2973/odp.proc.sr.117.133.1991>, 1991.
- Schefuß, E., Sinninghe Damsté, J. S., and Jansen, J. H. F.: Forcing of tropical Atlantic sea surface temperatures during the mid-Pleistocene transition, *Paleoceanography*, 19, PA4029, <https://doi.org/10.1029/2003PA000892>, 2004.
- Schiebel, R. and Hemleben, C.: *Planktic Foraminifers in the Modern Ocean*, Heidelberg: Springer Berlin, 358 pp., <https://doi.org/10.1007/978-3-662-50297-6>, 2017.
- Schlitzer, R.: Ocean Data View, AWI [code], <https://odv.awi.de> (last access: 12 March 2024), 2021.
- Shaffer, F. R.: The origin of the Walvis Ridge: sediment/basalt compensation during crustal separation, *Palaeogeogr. Palaeoclimatol.*, 45, 87–100, [https://doi.org/10.1016/0031-0182\(84\)90111-1](https://doi.org/10.1016/0031-0182(84)90111-1), 1984.
- Shannon, L. V. and Nelson, G.: The Benguela: large scale features and processes and system variability, in: *The South Atlantic*, edited by: Wefer, G., Berger, W. H., Siedler, G., and Webb, D. J., Springer-Verlag, Berlin, 163–210, ISBN 978-3-642-80355-0, 1996.
- Shannon, L. V., Boyd, A. J., Brundrit, G. B., and Taunton-Clark, J.: On the existence of an El Niño-type phenomenon in the Benguela System, *J. Mar. Res.*, 44, 495–520, 1986.
- Singh, A. K. and Sinha, D. K.: Northward Migration of Antarctic Polar Front During the Quaternary: Planktic Foraminiferal Record from Southeast Indian Ocean, *Journal of Climate Change*, 7, 13–24, <https://doi.org/10.3233/JCC210002>, 2021.
- Snyder, S. W. and Huber, B. T.: Preparation techniques for use of foraminifera in the classroom, *The Paleontological Society Papers*, 2, 231–236, 1996.
- Sokal, R. R. and Rohlf, F. J.: *Biometry*, 3rd edn., New York: W. H. Freeman and Company, ISBN 978-0716724117, 1995.
- Stramma, L. and England, M.: On the water masses and mean circulation of the South Atlantic Ocean, *J. Geophys. Res.*, 104, 20863–20883, <https://doi.org/10.1029/1999JC900139>, 1999.
- Stramma, L. and Peterson, R.G.: The South Atlantic Current, *J. Phys. Oceanogr.*, 20, 846–859, [https://doi.org/10.1175/1520-0485\(1990\)020<0846:TSAC>2.0.CO;2](https://doi.org/10.1175/1520-0485(1990)020<0846:TSAC>2.0.CO;2), 1990.
- Takayama, T. and Sato, T.: Coccolith biostratigraphy of the North Atlantic Ocean, DSDP Leg 94, in: *Initial Reports DSDP 94*, Washington (U. S. Govt. Printing Office), edited by: Ruddi-

- man, W. F., Kidd, R. B., Baldauf, J. G., Clement, B. M., Dolan, J. F., Eggers, M. R., Hill, P. R., Keigwin Jr., L. D., Mitchell, M., Philipps, I., Robinson, F., Salehipour, S. A., Takayama, T., Thomas, E., Unsold, G., and Weaver, P. P. E., 94, 651–702, <https://doi.org/10.2973/dsdp.proc.94.113.1987>, 1987.
- Talley, L. D.: Shallow, intermediate, and deep overturning components of the global heat budget, *J. Phys. Oceanogr.*, 33, 530–560, [https://doi.org/10.1175/1520-0485\(2003\)033<0530:SIADOC>2.0.CO;2](https://doi.org/10.1175/1520-0485(2003)033<0530:SIADOC>2.0.CO;2), 2003.
- Thiede, J.: Variations in coiling ratio of Holocene planktonic foraminifera, *Deep-Sea Res.*, 18, 823–831, [https://doi.org/10.1016/0011-7471\(71\)90049-0](https://doi.org/10.1016/0011-7471(71)90049-0), 1971.
- Thoram, S., Sager, W. W., Gaastra, K., Tikoo, S. M., Carvallo, C., Avery, A., Del Gaudio, A. V., Huang, Y., Hoernle, K., Höfig, T. W., Bhutani, R., Buchs, D. M., Class, C., Dai, Y., Dalla Valle, G., Fielding, S., Han, S., Heaton, D. E., Homrighausen, S., Kubota, Y., Li, C.-F., Nelson, W. R., Petrou, E., Potter, K. E., Pujatti, S., Scholpp, J., Shervais, J. W., Tshiningayamwe, M., Wang, X. J., and Widdowson, M.: Nature and origin of magnetic lineations within Valdivia Bank: Ocean plateau formation by complex seafloor spreading, *Geophys. Res. Lett.*, 50, e2023GL103415, <https://doi.org/10.1029/2023GL103415>, 2023.
- Ufkes, E. and Kroon, D.: Sensitivity of south-east Atlantic planktonic foraminifera to mid-Pleistocene climate change, *Palaeontol.*, 55, 183–204, <https://doi.org/10.1111/j.1475-4983.2011.01119.x>, 2012.
- Ufkes, E., Jansen, J. H. F., and Schneider, R. R.: Anomalous occurrences of *Neoglobobulimina pachyderma* (left) in a 420-ky upwelling record from Walvis Ridge (SE Atlantic), *Mar. Micropaleontol.*, 40, 23–42, 2000.
- van Leeuwen, R. J. W.: Sea-floor distribution and Late Quaternary faunal patterns of planktonic and benthic foraminifera in the Angola Basin, *Utrecht Micropaleontological Bulletins*, 38, 287 pp., 1989.
- Villar, E., Farrant, G. K., Follows, M., Garczarek, L., Speich, S., Audic, S., Bittner, L., Blanke, B., Brum, J. R., Brunet, C., Cassetto, R., Chase, A., Dolan, J. R., d’Ortenzio, F., Gattuso, J. P., Grima, N., Guidi, L., Hill, C. N., Jahn, O., Jamet, J. L., Le Goff, H., Lepoivre, C., Malviya, S., Pelletier, E., Romagnan, J. B., Roux, S., Santini, S., Scalco, E., Schwenck, S. M., Tanaka, A., Testor, P., Vannier, T., Vincent, F., Zingone, A., Dimier, C., Picheral, M., Searson, S., Kandels-Lewis, S.; Tara Oceans Coordinators; Acinas, S. G., Bork, P., Boss, E., de Vargas, C., Gorsky, G., Ogata, H., Pesant, S., Sullivan, M. B., Sunagawa, S., Wincker, P., Karsenti, E., Bowler, C., Not, F., Hingamp, P., and Iudicone, D.: Environmental characteristics of Agulhas rings affect interocean plankton transport, *Science*, 348, 1261447, <https://doi.org/10.1126/science.1261447>, 2015.
- Wade, B. S. and Bown, P. R.: Calcareous nannofossils in extreme environments: the Messinian salinity crisis, Poles Basin, Cyprus, *Palaeogeogr. Palaeoclimatol.*, 233, 271–286, <https://doi.org/10.1016/j.palaeo.2005.10.007>, 2006.
- Wade, B. S., Pearson, P. N., Berggren, W. A., and Pälike, H.: Review and revision of Cenozoic tropical planktonic foraminiferal biostratigraphy and calibration to the geomagnetic polarity and astronomical time scale, *Earth-Sci. Rev.*, 104, 111–142, <https://doi.org/10.1016/j.earscirev.2010.09.003>, 2011.
- Wade, B. S., Olsson, R. K., Pearson, P. N., Huber, B. T., and Berggren, W. A. (Eds.): *Atlas of Oligocene Planktonic Foraminifera*. Cushman Foundation Special Publication No. 46, 528 pp., 2018.
- Walter, H.: Die ökologischen Verhältnisse in der Namibnebelwüste (Südwestafrika) unter Auswertung der Aufzeichnungen des Dr. G. Boss (Swakopmund), in: *Jahrbücher für Wissenschaftliche Botanik*, edited by: Pringsheim, N., Leipzig, Gebrüder Borntraeger, 58–222, 1937.
- Wang, L.: Isotopic signals in two morphotypes of *Globigerinoides ruber* (white) from the South China Sea: implications for monsoon climate change during the last glacial cycle, *Palaeogeogr. Palaeoclimatol.*, 161, 381–394, [https://doi.org/10.1016/S0031-0182\(00\)00094-8](https://doi.org/10.1016/S0031-0182(00)00094-8), 2000.
- Wei, W.: Calibration of upper Pliocene–lower Pleistocene nannofossil events with oxygen isotope stratigraphy, *Paleoceanography*, 8, 85–99, <https://doi.org/10.1029/92PA02504>, 1993.
- Werner, R., Hoernle, K., Barckhausen, U., and Hauff, F.: Geodynamic evolution of the Galápagos hot spot system (Central East Pacific) over the past 20 m.y.: Constraints from morphology, geochemistry, and magnetic anomalies, *Geochem. Geophys. Geosyst.*, 4, 1108, <https://doi.org/10.1029/2003GC000576>, 2003.
- West, S., Jansen, J. H. F., and Stuut, J.-B.: Surface water conditions in the Northern Benguela Region (SE Atlantic) during the last 450 ky reconstructed from assemblages of planktonic foraminifera, *Mar. Micropaleontol.*, 51, 321–344, <https://doi.org/10.1016/j.marmicro.2004.01.004>, 2004.
- Wilson, J. T.: Submarine Fracture Zones, Aseismic Ridges and the International Council of Scientific Unions Line: Proposed Western Margin of the East Pacific Ridge, *Nature*, 207, 907–911, <https://doi.org/10.1038/207907a0>, 1965.
- Young, J. R.: Size variation of Neogene *Reticulofenestra* coccoliths from Indian Ocean DSDP cores, *Micropaleontology*, 9, 71–85, <https://doi.org/10.1144/jm.9.1.71>, 1990.
- Young, J. R.: Neogene, in: *Calcareous Nannofossil Biostratigraphy*, edited by: Bown, P. R., Chapman and Hall, Cambridge, 225–265, ISBN 0 412 78970 1, 1998.
- Young, J. R. and Bown, P. R.: Nannotax3 website, International Nannoplankton Association, <https://www.mikrotax.org/Nannotax3/> (last access: 15 January 2024), 2017.